

# Pace of Landscape Change and Pediment Development in the Northeastern Sonoran Desert, United States

Phillip H. Larson,\* Scott B. Kelley,<sup>†</sup> Ronald I. Dorn,<sup>†</sup> and Yeong Bae Seong<sup>‡</sup>

\*Department of Geography, Minnesota State University

<sup>†</sup>School of Geographical Sciences and Urban Planning, Arizona State University

<sup>‡</sup>Department of Geography Education, Korea University

Pediments of the Sonoran Desert in the United States have intrigued physical geographers and geomorphologists for nearly a century. These gently sloping bedrock landforms are a staple of the desert landscape that millions visit each year. Despite the long-lived scientific curiosity, an understanding of the processes operating on the pediment has remained elusive. In this study we revisit the extensive history of pediment research. We then apply geospatial, field, and laboratory cosmogenic <sup>10</sup>Be nuclide dating and back-scattered electron microscopy methods to assess the pace and processes of landscape change on pediment systems abutting the Salt River in Arizona. Our study focuses on the Utery pediments linked to base-level fluctuations (river terraces) of the Salt River. Relict pediment surfaces were reconstructed with dGPS data and kriging methodologies utilized in ArcGIS—based on preserved evidence of ancient pediment surfaces. <sup>10</sup>Be ages of Salt River terraces established a chronology of incision events, where calculating the volume between the reconstructed relict pediment and modern surface topography established minimum erosion rates (~41 mm/ka to ~415 mm/ka). Pediment area and length appear to have a positive correlation to erosion rate and development of planar pediment surfaces. Field and laboratory observations reveal that pediment systems adjust and stabilize at each Salt River terrace. Relief reduction across the pediment begins with pediment channel incision via headward erosion. Next, tributary drainage capture begins and collapses interfluves. Lateral stream erosion promotes planation where the porosity of decayed granite along channel banks exceeds the bedrock underneath ephemeral channels. *Key Words:* base level, desert geomorphology, landscape evolution, surface reconstruction, weathering.

美国索诺兰沙漠的山前侵蚀平原，困扰了自然地理和地形学者将近一个世纪。这些缓缓倾斜的床岩地形，是每年有数百万人造访的沙漠地景的主要产物。尽管存在着长足的科学好奇，但对于山前侵蚀平原进行的过程之理解却仍然相当晦涩。我们于本研究中，再次造访山前侵蚀平原研究的广泛历史。我们接着运用地理空间，田野，以及实验室的宇宙成因 <sup>10</sup>Be 核素测年法与背向散射电子显微镜方法，评估紧邻亚利桑那州盐河的山前侵蚀平原系统的地景变迁的速率与过程。我们的研究，聚焦连结至盐河基准面波动（河阶）的梅萨山前侵蚀平原。残余物的山前侵蚀平原表面，根据古老山前侵蚀平原表面所保存的证据，透过 Arc-GIS 所使用的 dGPS 数据和克利金方法进行再建构。盐河河阶的 <sup>10</sup>Be 定年，建立了切割事件的年代表，其中计算再建构的残余山前侵蚀平原和当代地表地形学之间的体积，建立了最小的侵蚀速率（~41 mm/ka 至 ~415 mm/ka）。山前侵蚀平原的面积和长度，似乎和侵蚀速率与平面山前侵蚀平原地表的发展具有正向相关性。田野与实验室的观察，揭露出山前侵蚀平原系统在每一个盐河河阶进行调节并使之稳定。山前侵蚀平原的地势缩减，从透过河道侵蚀的山前侵蚀平原河道切口开始。支流引流汲水接着发生，并使得河间地倾塌。横向的水流侵蚀，促进了夷平作用，其中沿着河岸衰退的花岗岩的多孔性，超越了短暂河道底下的床岩。 *关键词：* 基准面，沙漠地形学，地景演化，地表再建构，风化。

Los pedimentos del Desierto de Sonora en los Estados Unidos han intrigado a los geógrafos físicos y geomorfólogos durante casi un siglo. Estas geofomas rocosas ligeramente inclinadas son un componente básico del paisaje desértico que es visitado por millones cada año. No obstante, pese a una curiosidad científica de vieja data, la comprensión de los procesos que operan en el pedimento sigue siendo esquiva. En el presente estudio volvimos sobre la larga historia de la investigación pedimentana. Después, aplicamos datación cosmogénica de nucleido <sup>10</sup>Be geoespacial, de campo y laboratorio, y métodos de microscopía electrónica de barrido para evaluar el ritmo y los procesos de cambio del paisaje en sistemas pedimentanos contiguos al Río Salado, en Arizona. Nuestro estudio está centrado en los pedimentos de Utery que están conectados con las fluctuaciones del nivel de base (terrazas fluviales) del Río Salado. Se reconstruyeron superficies pedimentanas relictas con datos dGPS y metodologías kriging que se utilizan en Arc-GIS—con base en la evidencia preservada en antiguas superficies pedimentanas. Las edades <sup>10</sup>Be de las terrazas del Río Salado establecieron una cronología de eventos de

incisión, donde, al calcular el volumen entre el pedimento relicto reconstruido y la topografía de superficie moderna, establecieron tasas de erosión mínimas ( $\sim 41$  mm/ka a  $\sim 415$  mm/ka). El área y la longitud del pedimento parecen tener una correlación positiva con la tasa de erosión y el desarrollo de superficies planas del pedimento. Las observaciones de campo y laboratorio revelan que los sistemas del pedimento se ajustaron y estabilizaron en cada terraza del Río Salado. La reducción del relieve a través del pedimento empieza con la incisión de cauces en el pedimento por medio de erosión antecedente. Después, empieza la captura de drenajes tributarios y el colapso de los interfluvios. La erosión lateral de las corrientes induce al aplanamiento, donde la porosidad del granito en desintegración a lo largo de los bancos del cauce sobrepasa los efímeros cauces de la roca madre subyacente. *Palabras clave:* nivel de base, geomorfología de desierto, evolución del paisaje, reconstrucción de la superficie, intemperismo.

William Morris Davis helped found the American Association of Geographers (AAG), serving as its first president in 1904 and 1905 (Daly 1944). Davis is best known for his research on the role of base-level fall of rivers (Powell 1875) in setting off a “cycle of erosion” (Davis and Synder 1898; Davis 1902). Later in life, Davis developed a fascination with desert granitic landscapes, including erosional landforms known as pediments (Davis 1933, 1938). Ironically, despite a lengthy discussion of “dissected rock floors,” Davis paid little attention to the importance of base level on pediments—an issue that recent work (Gunnell et al. 2007; Strudley and Murray 2007; Larson et al. 2014) highlighted as a need for further analysis.

Since Davis’s time, AAG journals have published numerous papers on pediments and the associated mountain front (Bryan 1940; Tator 1952; Tuan 1962; Ruhe 1964; Butzer 1965; Holzner and Weaver 1965; Rahn 1967; Rognon 1967; Ongley 1974; Churchill 1981; Twidale and Mueller 1988; Friend 2000). More broadly, since Gilbert (1877) first analyzed planation surfaces in the Henry Mountains of Utah, geomorphologists have exhibited a fascination for the genesis of pediments (King 1949; Mabbutt 1966, 1977; Oberlander 1972, 1974; Cooke and Warren 1973; Büdel 1982; Twidale 1983; Dohrenwend and Parsons 2009)—but still currently struggle in understanding their long-term development, sometimes referred to as the “pediment problem” (Howard 1942; Oberlander 1974).

Physical geographers often use the descriptive term *piedmont*, named for a district of Italy, to denote low-gradient planar landforms fronting mountain ranges. In arid regions, piedmonts typically originate from either the deposition of alluvial fans or the erosion of bedrock that produces pediments with the same rock type as the backing mountain front (Oberlander 1989). As in any lengthy literature on a landform, variants and various terms emerged, including pediment domes (Davis 1933), dissected pediments (Koschmann and Loughlin 1934), soft-rock pediments (Schumm 1962), terrace pediments

(Barsch and Royse 1972; Plakht, Patyk-Kara, and Gorelikova 2000), apron pediments (Cooke and Warren 1973), pediplains (Twidale and Bourne 2013), pediments mantled with alluvium (Mabbutt 1977; Oberlander 1979; Twidale 1982; Applegarth 2004), and pediment flatirons (Schmidt 1989).

The most comprehensive review of pediments as a desert landform concluded:

There is a large literature on pediments. This literature has provided a wealth of information on the form of pediments and the settings in which they are found. We know much about the character and variability of pediments. In contrast, information about pediment processes is notably less. Even setting aside the difficult problem of the relationship of contemporary processes to pediment development, knowledge of these processes, *per se*, and their significance for contemporary sediment budgets in deserts is weak, and much needs to be done. (Dohrenwend and Parsons 2009, 408)

Convention holds that the pediment form represents the effects of mountain-front slope retreat, perhaps aided by isostatic rebound (Pelletier 2010), and sufficient sediment transport to maintain a bedrock platform over timescales of millions of years. Although our findings are not in conflict with this conventional view, we take a different approach to the study of rock pediments by combining modern methodological techniques of geographic information systems (GIS), differentially corrected Global Positioning System (dGPS), electron microscopy, and cosmogenic nuclide dating, with traditional field interpretations. In the north-central Sonoran Desert, tectonically inactive for the last 5 million years (Menges and Pearthree 1989), we measure rates of erosion as the ephemeral washes of arid granitic pediments respond to base-level lowering (Péwé 1978; Larson et al. 2014). These data support the hypothesis that processes responsible for pediment erosion in response to changing base level can mimic rates of landscape change found in tectonically active regions and generate newly formed pediments on the timescale of the last glacial cycle (last

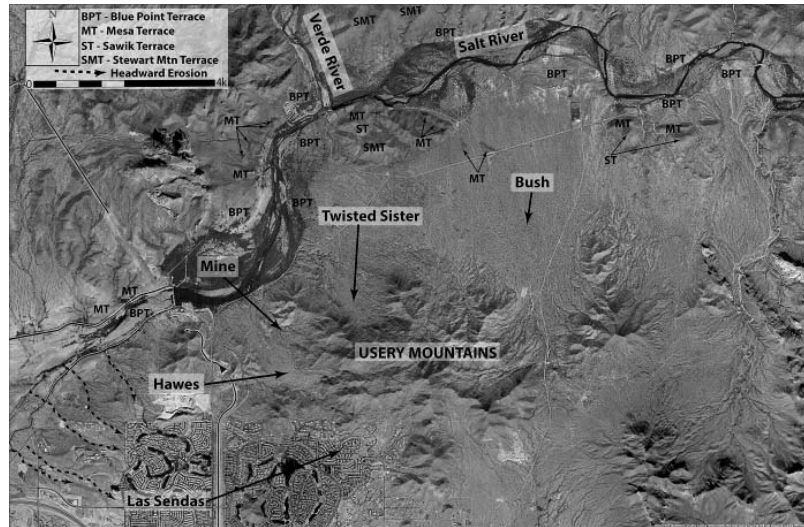


**Figure 1.** The lower Salt River valley and Usery Mountains. Here the five pediments and dissected pediments of the Usery Mountains draining to the Salt River form the key study areas for the geospatial reconstruction of relict pediment surfaces: Hawes dissected pediment, Mine dissected pediment, Twisted Sister dissected pediment, Bush pediment, and Las Sendas pediment. Other abbreviations note the terraces of the lower Salt River valley. They are, from highest to lowest: Stewart Mountain Terrace (Larson et al. 2010), Sawik Terrace (Péwé 1978), Mesa Terrace (Péwé 1978), and Blue Point Terrace (Péwé 1978). SMT = Stewart Mountain Terrace; ST = Sawik Terrace; MT = Mesa Terrace; BPT = Blue Point Terrace.

90,000 years). This article thus challenges the perception that rock pediments necessarily exemplify a stable desert landscape created by mountain-front retreat. Instability of the pediment toe can also induce pedimentation.

### Northeastern Sonoran Desert: A Unique Study Area

The Sonoran Desert represents a classic area for the study of pediments in North America (Bryan 1925; Ives 1936; Balchin and Pye 1956; Tuan 1962; Mammerickx 1964; Birot and Dresch 1966; Rahn 1967; Cooke 1970a; Barsch and Royse 1972; Kirkby and Kirkby 1974; Kesel 1977; Péwé 1978; Parsons and Abrahams 1984; Palm 1986; Liu et al. 1996; Bezy 1998; Applegarth 2004; Pelletier 2010). Whereas some mountain drainages erode enough sediment to form depositional piedmonts called alluvial fans, many Sonoran Desert ranges contain tiny basins and small washes that serve as conveyor belts transporting sandy and gravel detritus across low-sloping bedrock pediments.

Throughout the Sonoran Desert many formerly hydrologically closed basins now contain through-flowing river systems (Menges and Pearthree 1989). This change from endorheic to integrated basins dramatically influences the erosional and sedimentation histories of a landscape.

The establishment of rivers through these basins tied piedmont landforms bounding these basins to the base level created by the rivers. Whether by coincidence or an unstated preference, prior research in the southwestern United States often studied pediments draining into closed basins with slowly rising base levels (Howard 1942; Denny 1967; Twidale 1967; Oberlander 1972, 1974; Wells et al. 1985; Pelletier 2010). In contrast, pediments flanking through-flowing rivers in the Sonoran Desert (e.g., Agua Fria, Bull Williams, Gila, Salt, San Pedro, Verde) experienced a variety of base-level fluctuations—indicated by flights of fluvial terraces flanking these rivers (Péwé 1978).

The Salt River valley is an example of this story (Figure 1). This region first experienced aggradation, followed by multiple base-level declines (Péwé 1978; Douglass et al. 2009; Larson et al. 2010; Larson et al. 2014). The locations of the geologic and geomorphic features in the study area (Figure 1) derive from a combination of geologic mapping projects (Skotnicki and Leighty 1997; Pearthree et al. 2015), guidebooks (Péwé 1978), thesis research (Kokalis 1971; Pope 1974; Block 2007), and geomorphic research (Larson et al. 2010; Larson et al. 2014).

Each time the Salt River stabilized at a new base level, floodplains developed—serving as a local base level for adjacent ephemeral washes flowing across pediments.

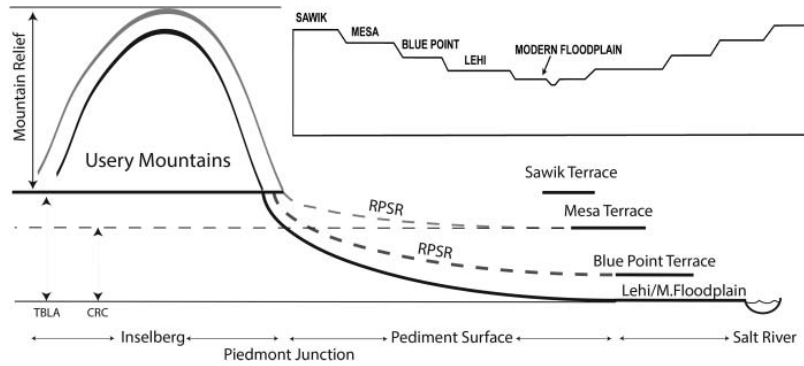


**Figure 2.** Pediment surfaces exist in a continuum of associated landforms (Dohrenwend and Parsons 2009). Former pediment surfaces once graded to the Sawik strath terrace; however, no evidence remains of this former pediment. In contrast, abundant remnants exist of the pediment that once graded to Mesa strath terrace (Larson et al. 2014). RPSR = relict pediment surface graded to an ancestral base level; TBLA = total base-level adjustment; CRC = calculated rate of change of pediments between two different base levels.

Conceptually, the evolution of this landscape is represented in the cross section in Figure 2. For example, much of the city of Mesa, Arizona, occupies the Mesa terrace, and the Las Sendas pediment still transitions downslope to this terrace (Figure 3A). The Bush pediment, in contrast, closely flanks the modern Salt River and is a relatively smooth pediment surface that transitions into the Blue Point terrace and the modern Salt River

(Figure 3B). Between the Bush and Las Sendas pediments are the Twisted Sister, Mine, and Hawes dissected pediments (Figure 4) that host abundant evidence of a formerly active pediment surface preserved above the modern pediment channels. Three specific types of evidence record the minimum elevation of this now abandoned pediment surface: laminar calcrete, uneroded pediment mantles, and zones of enhanced weathering

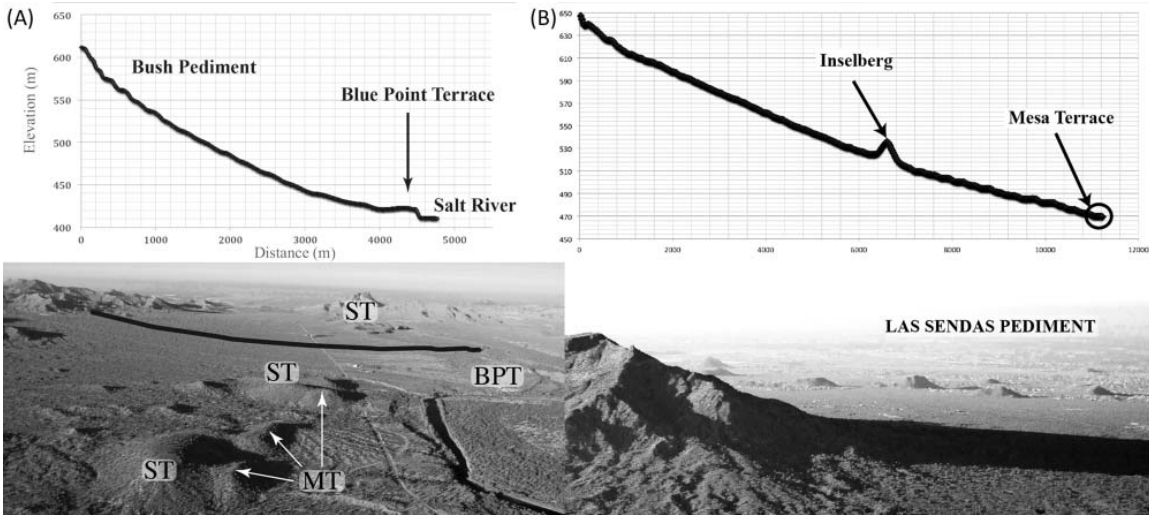


**Figure 3.** The classic shape of Usery Mountain pediments adjust and stabilize to two base levels. (A) The Bush pediment on the north side of the Usery Mountains transport grus to the Blue Point Terrace of the Salt River. The Bush pediment’s strikingly smooth form is a result of nearly complete repedimentation. Recent ongoing adjustment to base-level lowering from the BPT to the modern floodplain can be observed in the distal portion of the pediment. (B) The Las Sendas pediment on the southwestern side of the Usery Mountains still transports grus to the Mesa Terrace of the Salt River, a terrace that rests nearly 70 m above the modern river, with a number of small, ephemeral channels eroding headward into the distal end of this pediment (see Figure 1). Although the MT still represents the base level of the Las Sendas pediment, the other pediments are adjusting to the floodplain of the Salt River. Remnants of the Mesa-aged pediment surface still exist on the Bush, Twisted Sister, Mine, and Hawes pediments to varying degrees (Larson et al. 2014). MT, BPT, and ST denote terrace remnants next to the Salt River. BPT = Blue Point Terrace; ST = Sawik Terrace; MT = Mesa Terrace.

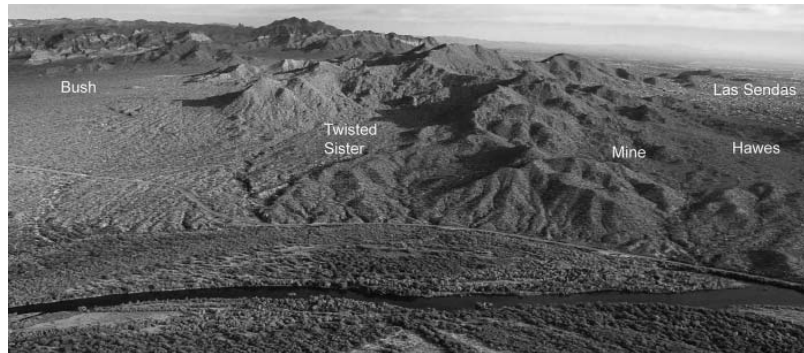


**Figure 4.** Oblique aerial photograph of the pediments and dissected pediments of the Utery Mountains investigated in this study.

(Larson et al. 2014). We introduce here the concept of a *relict pediment surface* as this former, now abandoned pediment level (Figure 2). The focus of this research rests in using these relict surfaces within the lower Salt River valley to estimate rates of change among the different pediment and dissected pediment systems of the Utery Mountains.

To develop a better understanding of the pace of change in these Sonoran Desert pediments, we frame our research on the conceptual model presented in Figure 2 by (1) measuring the ages of the Salt River's stream terraces using the buildup of  $^{10}\text{Be}$  in terrace cobbles because these terraces represent the base level of the relict pediment surfaces; (2) gathering dGPS data on the location and elevation of the different types of relict pediment indicators (Larson et al. 2014); (3) using ArcGIS software (various versions, Esri, Redlands, CA, USA) to quantify the minimum amount of landscape change between relict and modern pediments; (4) undertaking laboratory measurements of the state of decay of the bed and banks of pediment ephemeral washes; and (5) integrating these data with field interpretations and observations.

## Methods

### Cosmogenic $^{10}\text{Be}$ of Salt River Terraces

Terraces of the Salt River offer an ideal setting for cosmogenic nuclide dating through the buildup of  $^{10}\text{Be}$  in quartz cobbles because (1) strath terrace remnants provide a stable geomorphic surface with little evidence of postdepositional modification; (2) desert pavements on terrace surfaces form through flotation under accumulating dust (Pelletier, Cline, and DeLong 2007); and (3) fresh road and stream cuts offer

material to analyze the prior history of exposure to cosmic rays of the sampled alluvium. In particular, the Blue Point and Mesa terrace remnants selected for sampling display little topography with tight interlocking desert pavement development. Details on sampling locations are indicated in Table 1. Distance from escarpments and gullies minimizes postdepositional erosion. The sampled quartzite cobbles show little evidence of postdepositional modification, and sampling locations avoided any modern or paleo-evidence of bioturbation (Pietrasiak et al. 2014).

Six “disk-shaped” cobbles were collected from desert pavements on top of each terrace, thus yielding six different  $^{10}\text{Be}$  exposure ages for each terrace. Disk-shaped cobbles in desert pavements maintain their position on the surface through three processes: (1) overland flow removing fines (Sharon 1962; Cooke 1970b; Parsons, Abrahams, and Simanton 1992); (2) flotation as dust accumulates underneath the cobbles (Mabbutt 1977, 1979; McFadden, Wells, and Jercinovich 1987; Wells et al. 1995), where the disk shape traps dust efficiently underneath this flattened shape (Goossens 1995); and (3) dispersive stress from wetting and drying of clays underneath the cobbles (Springer 1958; R. W. Jessup 1960; Cooke 1970b). The net effect of these processes maintains the position of the cobble at the surface (Pelletier, Cline, and DeLong 2007).

Terrace cobbles were first crushed and sieved to the 250 to 750 micrometer fraction and then treated typically with  $\text{HF-HNO}_3$  to remove meteoric beryllium and organic matter (Kohl and Nishiizumi 1992). Following dissolution with a low ( $<10^{-15}$  in  $^{10/9}\text{Be}$ ) resolution  $^9\text{Be}$  carrier, Be is separated by ion exchange and precipitated at  $\text{pH} > 7$ . Beryllium hydroxides are dried and oxidized at  $800^\circ\text{C}$  for ten minutes by ignition in a quartz crucible.  $\text{BeO}$  is then mixed with Nb and loaded

**Table 1.**  $^{10}\text{Be}$  ages for Blue Point and Mesa terraces

Sample	Coordinates	Elevation (m)	Thickness (cm) <sup>a</sup>	Shielding factor <sup>c</sup>	$^{10}\text{Be}$ concentration ( $10^5$ atoms $\text{g}^{-1}\text{SiO}_2$ ) <sup>d</sup>	Exposure age (ka) <sup>e</sup>
Mesa001	33.53996, -111.62935	461	4	0.99	$7.70 \pm 0.28$	$91.5 \pm 8.8$
Mesa002	33.53988, -111.62924	462	5.5	0.99	$6.83 \pm 0.87$	$76.3 \pm 11.9$
Mesa003	33.53999, -111.62936	459	5	0.99	$6.19 \pm 0.37$	$64.3 \pm 6.8$
Mesa004	33.53991, -111.62922	458	4.5	0.99	$7.09 \pm 0.45$	$80.8 \pm 8.9$
Mesa005	33.53992, -111.62933	460	4.5	0.99	$7.88 \pm 0.46$	$95.4 \pm 10.2$
Mesa006	33.53999, -111.62952	458	4	0.99	$9.68 \pm 0.50$	$129.24 \pm 13.5$
Mesa007	33.53951, -111.62856	450	Deep <sup>b</sup>		$2.67 \pm 0.09$	Inheritance
BluePoint008	33.55286, -111.57689	434	3.5	0.99	$3.33 \pm 0.30$	$35.3 \pm 4.4$
BluePoint010	33.55286, -111.57689	434	4.6	0.99	$3.26 \pm 0.19$	$34.2 \pm 3.6$
BluePoint011	33.55286, -111.57689	434	4	0.99	$5.05 \pm 0.27$	$67.6 \pm 7.0$
BluePoint012	33.55286, -111.57689	434	5.8	0.99	$3.25 \pm 0.24$	$34.3 \pm 3.9$
BluePoint013	33.55286, -111.57689	434	5.4	0.99	$2.47 \pm 0.19$	$19.8 \pm 2.3$
BluePoint014	33.55286, -111.57689	429	Deep <sup>b</sup>		$1.40 \pm 0.08$	Inheritance

Note: The tops of all samples were exposed at the terrace surface.

<sup>a</sup>Whole cobble was used considering possible turnaround since initial deposition.

<sup>b</sup>Amalgamated ( $n > 30$ ) cobbles were sampled from deep ( $> 5$  m) depth.

<sup>c</sup>Geometric shielding correction for topography was measured on an interval of 10.

<sup>d</sup>Uncertainties are reported at the  $1\sigma$  confidence level. Propagated uncertainties include error in the blank, carrier mass (1%), and counting statistics.

<sup>e</sup>All ages are corrected for inheritance and expressed with  $1\sigma$  external uncertainty. Beryllium-10 model ages were calculated with the Cosmic-Ray Produced Nuclide Systematics on Earth online calculator version 2.2 (<http://hess.ess.washington.edu/>). Propagated error in the model ages include a 6 percent uncertainty in the production rate of  $^{10}\text{Be}$  and a 4 percent uncertainty in the  $^{10}\text{Be}$  decay constant.

into targets. 6MV accelerator mass spectrometry (AMS) at the Korea Institute of Science and Technology (KIST, Seoul, Korea) measured the targets (Kim et al. 2016). After blank ( $3 \times 10^{-15}$   $^{10}\text{Be}$ ) correction and normalization of isotope ratios to  $^{10}\text{Be}$  standards (Nishizumi et al. 2007) using a  $^{10}\text{Be}$  half-life of  $1.387 (\pm 0.03) \times 10^6$  year (Chmeleff et al. 2010; Korschinek et al. 2010), we converted measured ratios into an absolute ratio of  $^{10}\text{Be}/^9\text{Be}$  in quartz.

Inheritance produced during prior exposure was quantified from amalgamated cobbles ( $n > 30$ ) sampled from a depth where surface production of  $^{10}\text{Be}$  would not occur ( $> 5$  m). These cobbles were collected from a road cut and also a stream cut. The approaches of using subsurface samples to estimate the effects of prior inheritance (Anderson, Repka, and Dick 1996; Oskin et al. 2007; Owen et al. 2011; Huang et al. 2014) and sample amalgamation (Anders et al. 2005; Marchetti and Cerling 2005; Matmon et al. 2009; Guralnik et al. 2010; Fisher et al. 2014) are both common.

The exposure ages were calculated using the following equation (Lal 1991):

$$N_t = P_0 \left( 1 - e^{-(\lambda + \varepsilon/z^*)t} \right) / (\lambda + \varepsilon/z^*), \quad (1)$$

where  $N_t$  is measured concentration (atoms  $\text{g}^{-1} \text{yr}^{-1}$ ) after long exposure ( $t$ ) and  $P_0$  (atoms  $\text{g}^{-1} \text{yr}^{-1}$ )  $^{10}\text{Be}$

production rate at the surface, and  $\lambda$  ( $\text{yr}^{-1}$ ) is the decay constant of  $^{10}\text{Be}$ .  $\varepsilon$  means the denudation rate, and  $z^*$  is  $\Lambda/\rho$ , a depth scale of absorption mean free path where  $\Lambda$  is  $160 \text{ gcm}^{-2}$  and  $\rho$  is  $2.7 \text{ g/cm}^{-3}$ . We calculated  $^{10}\text{Be}$  exposure ages using the Cosmic-Ray Produced Nuclide Systematics exposure age calculator (version 2.2; Balco et al. 2008) by integrating shielding conditions, latitude–altitude production rate functions (Lal 1991; Stone 2000; Heisinger, Lal, Kubik, Ivy-Ochs, Knie, et al. 2002; Heisinger, Lal, Kubik, Ivy-Ochs, Neumaier, et al. 2002) applying  $4.49 \pm 0.39 \text{ g}^{-1} \text{yr}^{-1}$  at sea-level, high-latitude for the  $^{10}\text{Be}$  reference spallation production rate in this study (Stone 2000; Balco et al. 2008). Propagated error in the model ages includes a 6 percent uncertainty in the production rate of  $^{10}\text{Be}$  and a 4 percent uncertainty in the  $^{10}\text{Be}$  decay constant.

### Point Location Rates of Pediment Change

Salt River terrace remnants preserved above younger pediments provide an opportunity to calculate incision rates at specific locations. Altogether, we identified six of these places. By convention, erosion rates are typically presented in units of millimeters per thousand years (mm/ka). Calculating error terms involves the error of topographic measurements (the

standard deviation of elevation differences at ten locations) and the error term for cosmogenic ages. Calculating erosion rate error terms for points in the landscape uses the extremes (highest elevation difference/smallest age difference and lowest elevation difference/highest age difference). Each circumstance of older river terrace adjacent to younger pediment only offers insight into erosion rates at a specific location.

### Reconstruction Relict Surfaces

Our geospatial approach can be introduced as a thought exercise using Figure 2, where our objective rests in measuring the volume of the “slices” between the different relict pediment surfaces (RPSR) and the modern active pediment surface. Global Positioning System (GPS) data collection and GIS modeling facilitate (1) reconstruction of an RPSR; (2) calculation of the volume of eroded material between the RPSR and the modern pediment; (3) with  $^{10}\text{Be}$  ages, calculate minimum rates of erosion for entire pediments; and (4) interpret the significance of these minimum erosion rates with the aid of other data such as pediment lengths, pediment areas, and pediment drainage processes operating on the pediments.

Pediments draining the granitic Utery Mountains toward the Salt River contain remnants of former pediments, including (1) mantles of sandy grus in the process of eroding; (2) regolith carbonate formed at the contact between sandy grus and granitic bedrock; and (3) highly weathered bedrock where the pediment mantle met the backing bedrock inselberg slope. Previous research established that each remnant represents a minimum height of the now-eroded pediment (Larson et al. 2014). We mapped all remnants using a Trimble GeoPro XH dGPS with < 0.5 m vertical precision.

Reconstruction of relict surfaces required interpolation and kriging techniques to produce continuous surfaces of relict pediments. Kriging uses known points of reference and associated attribute values, and various statistical functions to interpolate unknown values away from the reference points (Oliver and Webster 1990). In our case, the value of interest is the relict surface elevation. Using kriging tools within the ArcGIS 10.1 Geostatistical Analyst (Esri, Redlands, CA, USA), we produced a number of different relict surfaces for each pediment age. Then, by clipping current digital elevation models (DEMs) to the pediment watershed boundaries, distinguished by notable drainage divides, a cut/fill analysis in ArcGIS calculated

volumetric differences between modern and relict surfaces. To ensure consistent extent and resolution between the two input surfaces, we generated interpolated relict surfaces at 10-m resolution to match the existing DEM.

The spherical model was fit to the empirical semivariogram for each of the four pediment surfaces, as this model best described the decay of spatial autocorrelation for the sampled GPS points. Sampling was restricted to sites where calcrete exposures could be found, mainly along ridgetops or on mountainsides, and we attempted to collect these points as dispersed as possible throughout the drainage basin. We performed ordinary kriging because  $\mu$  is unknown and we assume a constant trend of elevation change in the reconstructed surfaces. This also ensures that estimates of erosion rates constructed from the relict surfaces are as simplistic as possible. Surfaces are also anisotropic, with spatial autocorrelation higher at points along elevation contours compared to those along a pediment's longitudinal profile.

Even with this measure of consistency, variations in kriging techniques and parameters can produce varying surface types, introducing uncertainty into the output. Because our objective rests in calculating a minimum erosion rate for each pediment and dissected pediment surface (Hawes, Mine, Twisted Sister, and Bush in Figures 1 and 4), we focused on conservative assumptions. To standardize interpolation surfaces for all pediment systems to the greatest degree possible and maintain a simplistic model of the relict pediment, three key criteria were established based on the literature. These criteria had to be met before considering a relict surface as viable: (1) the surface had to represent a minimum erosion rate; (2) the surface had to reflect the general description of natural pediments in being a low relief—gently sloping surface, minimizing unnecessary transverse undulations; and (3) the surface had to minimize areas of volume gain between the relict and modern surfaces that might arise due to variability in the kriging techniques.

Once a relict surface met these criteria, we conducted a sensitivity analysis to create a margin of error for the erosion rate. Each kriging operation relies on a number of user-defined inputs, including the number of lag sizes, application of anisotropy (directional dependency), and minimum and maximum number of known reference points to consider for interpolation. Modifications to these inputs affected output erosion rates to a small degree. We compiled thirty systematic input parameter variations of each acceptable surface

to generate an erosion rate margin of error for each time interval in the analysis.

To estimate the erosion rates for each of the thirty surfaces generated, we divided the volumetric difference by the area and then divided again by the estimated age of the surface to reach rates in the units of millimeters per thousand years. For each surface, we entered three separate ages to obtain a composite margin error for the erosion rates based on the uncertainty in the sampled age of the surface: mean age (89,630 ka), and  $\pm 22,367$  ka. These calculations assumed a constant erosion rate for each relict surface. Recent concerns over the use of incision rates to understand tectonic or climatic unsteadiness in rivers (DiBiase 2014; Finnegan, Schumer, and Finnegan 2014; Gallen et al. 2015) are not crucial to this work in that we seek to measure total amount of erosional change in these pediments, as it pertains to each period of adjustment from stable base level to stable base level, from terrace tread to terrace tread.

### Measuring the Decay of Granite

The Utery Mountain pediments are composed of granitic lithologies. Because rates of erosion for granite depend on the state of rock decay (B. S. Jessup et al. 2011), and because partially gussified rock often characterizes granitic pediments (Mabbutt 1966; Oberlander 1974; Moss 1977; Twidale and Mueller 1988; Dohrenwend and Parsons 2009), we analyzed the state of granitic decay on the Utery pediments. Field-based strategies to analyze granitic decay remain flawed, because moisture can greatly affect the physical strength of grus (Wakatsuki et al. 2007). Thus, we employed measurements of porosity of bedrock granitic material, because greater internal porosity requires less shear stress to detach and erode grus (Ehlen and Wohl 2002; Ehlen 2005).

Samples were collected at evenly spaced intervals along the main ephemeral washes in each of the dissected pediments (Twisted Sister, Mine, Hawes). In addition, we gridded the Bush pediment and used a random number generator to select the grids for sampling washes to the closest center point of the grid. We measured bedrock porosity in three field contexts: bedrock in the middle of a pediment wash; along the bank of the wash; and then 80 to 100 cm into the bank, extracted by picking a trench into the bank and then backfilling after sampling.

Collected samples were polished for study with back-scattered electron (BSE) microscopy. Using

methods detailed previously (Dorn 1995), digital image processing of BSE imagery at a scale of  $1,000\times$  enables calculation porosity in rock material—in this case a cross-sectional area of  $2\text{ mm}^2$ . The reported porosity includes intramineral pores and pores along mineral–grain boundaries. Whereas porosity data are calculated to hundredths of a percent, a conservative solution in dealing with different pore types is to round off to the nearest tenth.

## Results

### Cosmogenic Ages of Salt River Terraces

Table 1 presents  $^{10}\text{Be}$  exposure ages for the Blue Point and Mesa terraces of the Salt River. The dated gravels accumulated  $^{10}\text{Be}$  prior to deposition on a floodplain, and we corrected ages for this prior exposure history. Then, additional  $^{10}\text{Be}$  accumulated in the gravels when the Salt River floodplain was abandoned by base-level lowering. These  $^{10}\text{Be}$  ages thus make it possible to estimate the length of time between shifts in base level of the Salt River and construct the chronology of significant basin-wide change. The  $89.6 \pm 22.4$  ka and  $38.3 \pm 17.6$  ka  $1\sigma$  ages for the Mesa and Blue Point terraces mean that the time between these two surfaces is best placed at 51.3 ka; considering the  $1\sigma$  errors, the age difference could be as little as 11.3 ka and as great as 91.3 ka. Thus, the  $1\sigma$  age difference between the Mesa and Blue Point base level is best interpreted as  $51.3 \pm 40$  ka. Then, the  $1\sigma$  time difference between the Blue Point terrace and the modern floodplain of the Salt River is  $38.3 \pm 17.6$  ka.

### Point Location Rates of Pediment Change

Each location in Table 2 offers insight into erosion rates between two time periods at a specific point location along a pediment flanking the Salt River. Regardless of the time interval involved or position with respect to the Salt River, we note that the central tendency of the different erosion rates all rest within a factor of two to three. These are not minimum rates of erosion, but rather rates based on intact fossil surfaces.

### Reconstructing Relict Pediment Surfaces and Calculating Rates of Change

Figures 5 and 6 present the boundaries of the Bush pediment and Mine, Hawes, and Twisted Sister

**Table 2.** Pediment erosion rate at locales where original surface exists

Coordinates	Erosion occurred between these time periods	Age $\delta$ (ka)	Elevation $\delta$ (m)	Incision rate (mm/ka)	1 $\sigma$ range (mm/ka)
33.547853, -111.728273	Mesa–Blue Point	51.3 $\pm$ 40	15 $\pm$ 1.3	292	150–1,442
33.538129, -111.577538	Mesa–Blue Point	51.3 $\pm$ 40	23.5 $\pm$ 2.5	458	230–2,301
33.543392, -111.584495	Mesa–Blue Point	51.3 $\pm$ 40	32 $\pm$ 4.1	624	305–3,195
33.539755, -111.628939	Mesa–modern	89.6 $\pm$ 22.4	22 $\pm$ 3.3	246	167–377
33.543438, -111.603865	Mesa–modern	89.6 $\pm$ 22.4	36 $\pm$ 4.0	402	286–595
33.525394, -111.692526	Mesa–modern	89.6 $\pm$ 22.4	31 $\pm$ 1.9	346	260–490

dissected pediments that are adjusting to the lowered base level of the Salt River. The generated relict surface DEM is portrayed in the gradient underlying the pediment boundary and overlying the satellite imagery of each pediment locale. These figures also present corresponding examples of relict pediment surface reconstruction. Table 3 summarizes the change between thirty modeled relict pediment surfaces and present-day pediment topography. It also summarizes the volume eroded and the erosion rates of the pediment and dissected pediments in Figures 1 and 4.

The modeled relict surfaces generate a range of erosion rates for the average  $^{10}\text{Be}$  age for the Mesa terrace and then also for  $1\sigma$  error of the  $^{10}\text{Be}$  age (Table 3). We stress that all erosion rates in Table 3 are minimums, because the calcrete, pediment mantle, and weathered zones used to create these surfaces all developed beneath the Mesa pediment surface (Larson et al. 2014). Pediment length and area both show a clear positive relationship with these minimum erosion rates (Figure 7).

#### Preparation for Erosion: Measuring Decay

Erosion of granitic pediments requires that the bedrock be in a sufficient state of decay to detach grus particles. Table 4 presents sampling locations and data on bedrock porosity in the bedrock of ephemeral channels, in the banks of ephemeral channels, and in the interior of these banks and its relationship to the widths of the washes. The ratio of porosity in the channel to the porosity in the bank represents a proxy for the erodability of the bedrock. Ratios greater than 1 indicate locations where banks are more resistant to erosion than channel floors, and Figure 8 shows that such spots generally host narrow washes. Figure 8 also illustrates that channels with ratios less than 1 are wider. After transforming channel width to  $\log_{10}$ , the linear regression has an  $r$  value of  $-0.67$  and is statistically significant at  $p < 0.05$  (Figure 8).

Field observations contextualize the data portrayed in Figure 8 and Table 4. Ephemeral pediment washes erode narrow incised channels into granite described as strongly weathered using Ehlen's (2005) classification (Figure 9A–C) and widen those channels where the channel floors are less porous and the banks are strongly weathered (Figure 9E–F). Thus, pediment washes appear to incise until they encounter granitic rock with less porosity and then they widen.

Factors other than the state of bedrock granite porosity also influence channel width. Locations immediately downstream of where larger pediment drainages converge often have significantly wider channels (Figure 10). Widening also occurs where ephemeral channels with larger drainage areas approach the base level of the Salt River after exiting a confined channel reach, such as where a wash cuts through a stream terrace or exits an incised channel.

#### Discussion

Base-level fluctuations of through-flowing rivers in the Sonoran Desert resulted when closed, internally drained basins integrated into through-flowing drainage networks (Menges and Pearthree 1989; Larson et al. 2010; Larson et al. 2014; Jungers and Heimsath 2015). Although most pediment research eschews settings with rapidly lowering base level, the pediments of the Salt River (Figure 4) represent the next step of pediment evolution in the Basin and Range physiographic province (Larson et al. 2014). We acknowledge, therefore, that some might consider the observations made here a special case and not relevant to pediments in closed basins. Furthermore, we acknowledge that some pediment development in our study area took place when the Utery Mountains were surrounded by closed basins; during this time frame, a number of functional models (e.g., Pelletier 2010) could explain pediment growth and how isostatic compensation from an eroding mountain mass might play a role.

We argue here, however, that the Salt River pediments offer the chance to see pedimentation

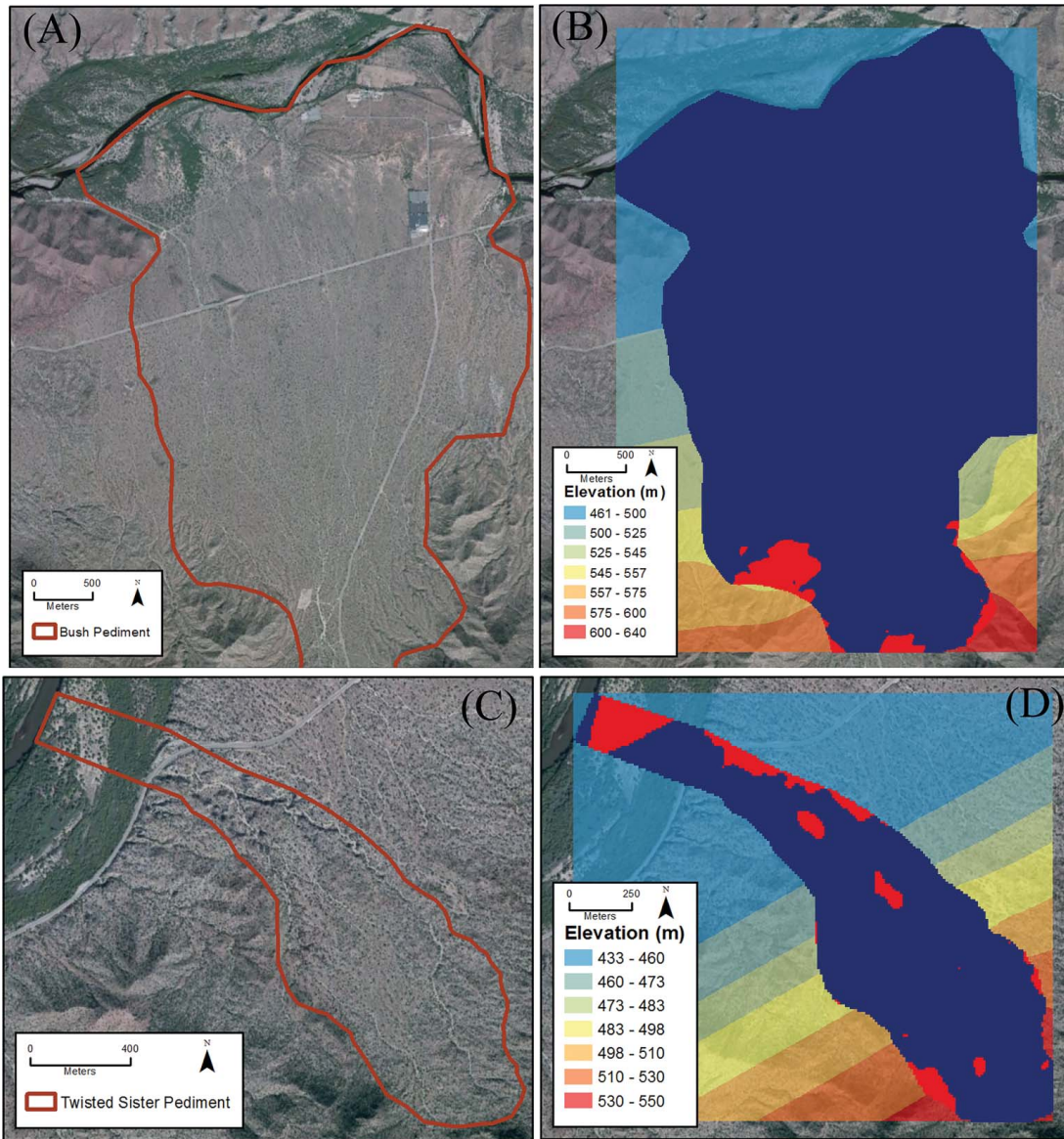


**Figure 5.** Red lines delineate the (A) Bush pediment and (C) Twisted Sister dissected pediment. In mapping the relict pediment surfaces (B and D), red areas indicate locations where the kriging methods generated elevations higher than the present-day topography. The kriging methods used minimized this gain. Blue colors map out the areas of denudation based on the models. The backdrop gradient in (B) and (D) represents the relict surface digital elevation model. (Color figure available online.)

processes in a greatly accelerated condition as the result of dynamic base-level fluctuation. Currently closed or endoreic basins, like those of the Great Basin in the United States, containing pediments that later become part of integrated river systems would also respond to changing base-level conditions in a pediment surface that is not in a steady state—where the different Utery pediments are in

transient states (Whipple 2004; Gran et al. 2013) adjusting to base-level fall.

#### Base Level as a Powerful Control on Pace of Change

Prior research into rates of pediment downwearing point to very slow erosion rates. K/Ar ages for lava

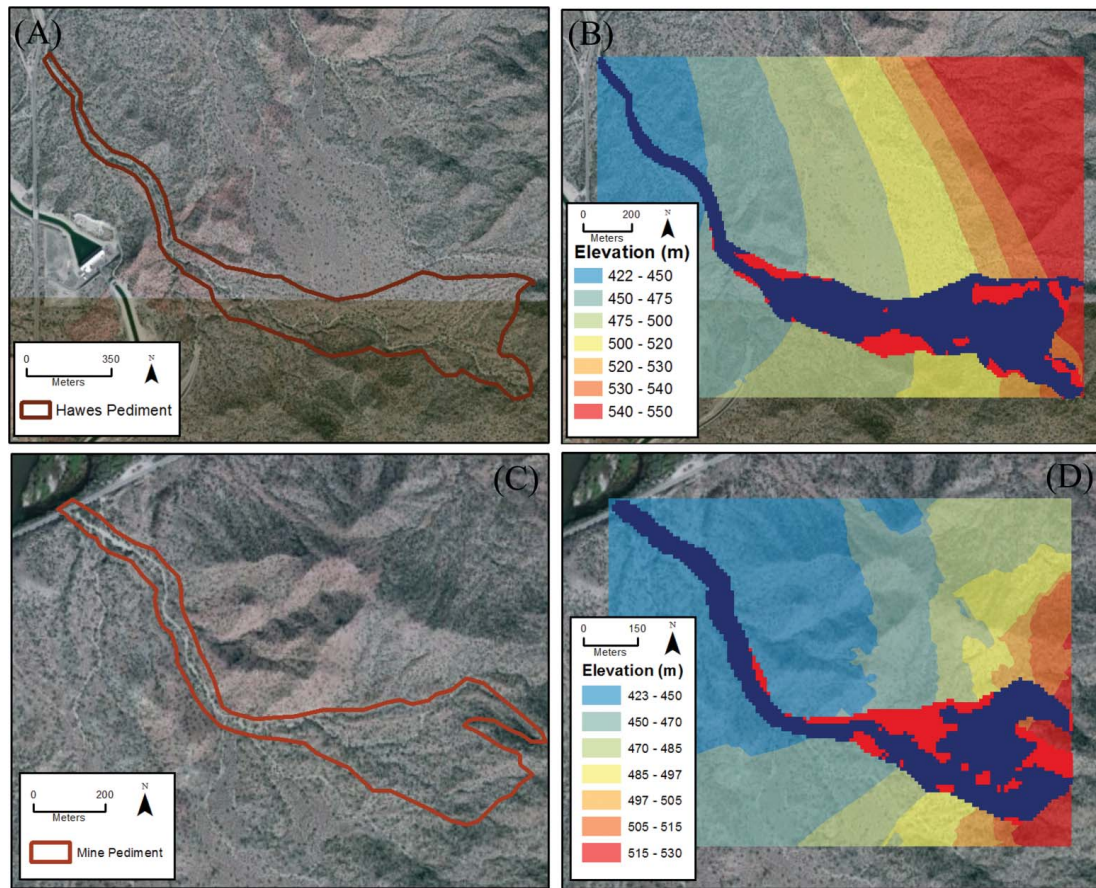


**Figure 6.** Red lines delineate the (A) Hawes and (C) Mine dissected pediments. In mapping the relict pediment surfaces (B and D), red areas indicate locations where the kriging methods generated elevations higher than the present-day topography. The kriging methods used minimized this gain. Blue colors map out the areas of denudation based on the models. The backdrop gradient in (B) and (D) represents the relict surface digital elevation model. (Color figure available online.)

flows capping pediments enable the calculation of erosion rates from the paleosurface under the lava to the present-day surface. Dohrenwend and Parsons (2009) summarized insight obtained from this approach in U.S. western areas of endoreic drainage where meters per million years is equivalent to millimeters per thousand years (mm/ka):

For several widely separated upland and piedmont areas within the Great Basin and Mojave Desert. For upland areas, these estimates range between 8 and 47 m per million years for periods of 0.85–10.8 m.y.; whereas for proximal piedmont areas, the estimates range from less than 2–13 m per million years for periods of 1.08–8.9 m.y. During similar time periods, medial piedmont areas have remained largely unchanged. These data document a general evolutionary scenario of upland downwearing and proximal piedmont regrading which has been regulated in part by the long-term stability of the medial

piedmont which serves as a local base level for the upper part of the pediment association. (394)

Cosmogenic  $^{10}\text{Be}$  and  $^{26}\text{Al}$  measurements are able to provide downwearing erosion rates for specific point locations on pediments for the last 0.1 to 1 million years of 10 to 21 mm/ka for the Chemeheuvi Mountains in the Mojave Desert (Nichols et al. 2005); 10 to 20 mm/ka for southern India (Gunnell et al. 2007); 7 mm/ka for a Namib Desert pediment surface (Bierman and Caffee 2001); 3.8 mm/ka for a tor in dissected pediment in southeastern Australia (Heimsath et al. 2001); 1 to 5 mm/ka for inselbergs backing granitic pediments in the Namib Desert (Cockburn, Seidl, and Summerfield 1999; Matmon et al. 2013);  $\sim 1$  mm/ka for an abandoned pediment in north-central Chile; and 0.11 to 3.2 mm/ka for dissected pediments in southern Africa (Bierman et al. 2014).

**Table 3.** Minimum erosion rates for Usery Mountain pediments

Pediment	Length (m)	Area (m <sup>2</sup> )	Average $\pm 1\sigma$ volume eroded (m <sup>3</sup> )	<sup>10</sup> Be age $\pm 1\sigma$	Erosion rate $\pm 1\sigma$ (mm/ka) <sup>a</sup>
Bush	4,764	13,182,100	489,737,252 $\pm 33,093,150$	-67.3 ka	552 $\pm$ 37
				<b>89.6 ka</b>	<b>415 <math>\pm</math> 28</b>
				+112 ka	332 $\pm$ 22
Twisted Sister	2,519	1,005,200	11,150,082 $\pm 2,228,202$	-67.3 ka	164 $\pm$ 33
				<b>89.6 ka</b>	<b>124 <math>\pm</math> 24</b>
				+112 ka	99 $\pm$ 20
Hawes	1,785	443,000	1,958,896 $\pm 846,449$	-67.3 ka	66 $\pm$ 28
				<b>89.6 ka</b>	<b>49 <math>\pm</math> 21</b>
				+112 ka	39 $\pm$ 17
Mine	1,593	209,800	773,368 $\pm 231,462$	-67.3 ka	54 $\pm$ 16
				<b>89.6 ka</b>	<b>41 <math>\pm</math> 12</b>
				+112 ka	32 $\pm$ 10

Note: <sup>a</sup>The erosion rate  $1\sigma$  errors are based on thirty different surface reconstruction models for three different age scenarios: the mean <sup>10</sup>Be age and also the  $\pm 1\sigma$  ages. Bold values represent mean age and erosion rate.

In contrast, our Salt River data reveal minimum erosion rates that are about five to thirty times faster (Tables 2 and 3) than the highest rates of erosion observed elsewhere in prior literature. Although the results in Table 2 for point locations provide the same sort of insight into downwearing rates as prior research, the minimum rate of erosion for an entire pediment or dissected pediment systems obtained through the geospatial strategy (Table 3) generates unique insight into an entire pediment. Even the slowest eroding Usery dissected pediments are eroding faster than the highest rates reported previously.

Unfortunately, all existing strategies to measure erosion rates suffer from the same limitation. Using K/Ar-dated lava flows or dated stream terraces (Table 2) to measure differences between two surfaces, using cosmogenic nuclide at point locations, and using geospatial subtraction of different surfaces (Table 3) all yield rates that can only be interpreted as linear constants. Neither our approach nor prior strategies are able to tease out changes in rates over time.

The rapidity of pediment adjustment observed along the Salt River can be placed in a broader comparative context. Usery pediment erosion rates fall

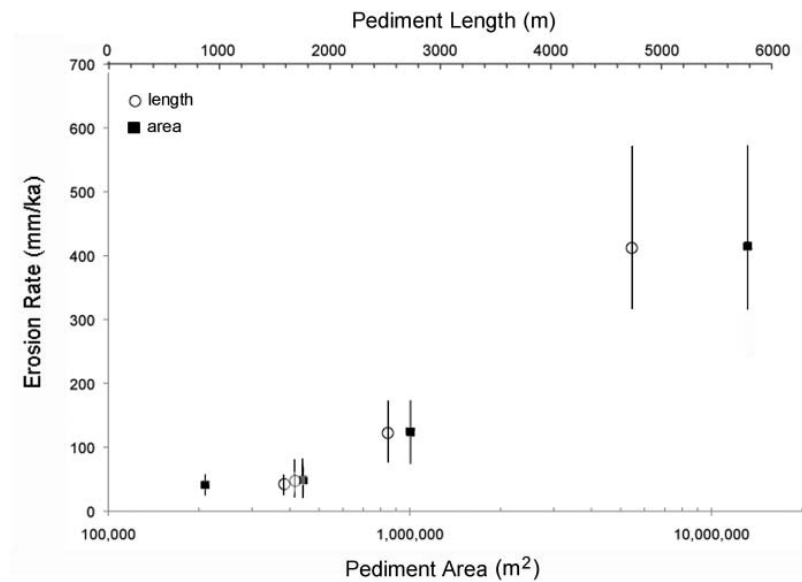


**Figure 7.** Scatterplots of minimum erosion rate (with  $1\sigma$  error) for the four pediments' plotted pediment length and area.

**Table 4.** Percent porosity of granodiorite in Usery Mountains pediments and dissected pediments

Pediment	Coordinates	Channel width (m)	% porosity at bank	% porosity in interior	% porosity channel	Depth to channel bedrock (m)	Ratio channel: bank porosity
Bush1	33.516543, -111.624178	4.9	22.0	14.9	25.1	0.1	1.1
Bush2	33.523176, -111.632643	2.2	30.1	25.2	29.7	0.3	1.0
Bush3	33.527240, -111.628881	4.7	49.5	24.7	22.0	0.4	0.4
Bush4	33.526587, -111.633702	3.2	40.5	19.4	20.5	0.3	0.5
Bush5	33.517542, -111.626916	0.9	20.6	17.5	36.2	0.0	1.8
Bush6	33.518842, -111.629446	0.6	21.1	20.6	29.1	0.0	1.4
Bush7	33.530811, -111.621466	3.1	85.6	33.2	22.1	1.2	0.3
Bush8	33.530358, -111.626661	0.8	26.0	22.8	33.9	0.1	1.3
Bush9	33.530302, -111.630150	6.1	55.8	41.4	24.3	0.9	0.4
Bush10	33.539263, -111.616865	4.5	62.0	35.3	21.0	1.1	0.3
Bush11	33.539899, -111.630447	1.1	18.3	22.4	37.7	0.0	2.1
Bush12	33.545800, -111.623507	6.6	72.7	40.6	23.8	0.8	0.3
Bush13	33.550084, -111.606869	1.4	19.9	20.2	31.0	0.0	1.6
Bush14	33.539893, -111.614657	5.3	75.4	55.0	26.9	1.3	0.4
Bush15	33.523888, -111.612262	5.9	48.8	40.9	27.4	0.7	0.6
Bush16	33.552134, -111.625216	13.6	59.4	55.3	30.6	1.2	0.5
Bush17	33.539242, -111.618441	1.3	55.8	51.0	31.4	1.8	0.6
Bush18	33.532356, -111.618505	7.7	61.3	57.6	28.0	1.7	0.5
Bush19	33.523605, -111.617631	5.8	60.3	56.7	30.5	2.0	0.5
Bush20	33.517657, -111.614670	7.0	63.2	59.3	31.3	1.5	0.5
Bush21	33.514052, -111.612090	3.3	24.2	22.7	29.8	0.0	1.2
Bush22	33.511693, -111.607341	2.2	22.8	19.9	28.4	0.1	1.2
TwistedSister1	33.522853, -111.663088	16.8	44.5	34.3	22.3	2.0	0.5
TwistedSister2	33.522132, -111.661228	10.8	33.1	28.4	20.2	1.8	0.6
TwistedSister3	33.521033, -111.658378	15.2	28.4	30.7	21.7	2.1	0.8
TwistedSister4	33.519845, -111.656952	1.4	22.5	19.6	18.4	0.0	0.8
TwistedSister5	33.518963, -111.656004	3.3	33.7	29.6	19.4	0.2	0.6
TwistedSister6	33.517634, -111.654865	8.2	37.0	35.3	22.1	1.2	0.6
TwistedSister7	33.515637, -111.654767	16.7	49.2	38.9	22.5	0.9	0.5
TwistedSister8	33.513657, -111.653508	6.4	26.7	27.5	20.6	0.6	0.8
TwistedSister9	33.512326, -111.652931	0.9	15.8	16.0	28.0	0.0	1.8
TwistedSister10	33.511956, -111.651951	0.6	16.0	17.2	26.9	0.0	1.7
TwistedSister11	33.511344, -111.651272	0.5	19.6	19.1	25.3	0.0	1.3
TwistedSister12	33.523456, -111.666464	25.2	36.3	25.4	N/A	> 2.5 m	N/A
TwistedSister13	33.523398, -111.665056	31.4	40.1	29.3	N/A	> 2.5 m	N/A
TwistedSister14	33.522416, -111.663307	6.7	36.2	28.2	23.7	1.9	0.7
TwistedSister15	33.520759, -111.662155	0.8	24.9	17.3	13.0	0.0	0.5
TwistedSister16	33.518770, -111.661046	6.5	30.5	25.9	22.8	0.8	0.7
TwistedSister17	33.517032, -111.660662	1.1	27.9	26.0	20.4	0.4	0.7
TwistedSister18	33.515232, -111.658712	6.9	31.0	28.2	23.5	0.2	0.8
TwistedSister19	33.513787, -111.656719	7.2	54.4	50.8	24.5	0.9	0.5
TwistedSister20	33.511879, -111.655284	8.3	44.3	36.7	22.2	0.3	0.5
TwistedSister21	33.510387, -111.654522	1.0	18.0	12.9	24.0	0.0	1.3
TwistedSister22	33.508974, -111.654667	0.5	16.7	11.0	22.7	0.0	1.4
TwistedSister23	33.506845, -111.654218	0.2	12.6	19.2	20.6	0.0	1.6
Mine1	33.515924, -111.676015	6.8	33.3	27.8	20.4	2.2	0.6
Mine2	33.514603, -111.673584	7.2	35.2	30.9	21.9	1.8	0.6
Mine3	33.512999, -111.672919	13.4	35.2	30.0	21.3	1.1	0.6
Mine4	33.510924, -111.671428	13.9	37.0	33.5	22.8	1.3	0.6
Mine5	33.510548, -111.668370	5.7	28.1	24.7	22.6	0.2	0.8
Mine6	33.510432, -111.666584	2.9	26.9	23.3	19.0	0.1	0.7
Mine7	33.510282, -111.664669	0.3	18.4	18.1	25.9	0.0	1.4

(Continued on next page)

**Table 4.** Percent porosity of granodiorite in Userly Mountains pediments and dissected pediments (*Continued*)

Pediment	Coordinates	Channel width (m)	% porosity at bank	% porosity in interior	% porosity channel	Depth to channel bedrock (m)	Ratio channel: bank porosity
Hawes1	33.509888, -111.682960	5.0	22.4	27.8	26.0	0.1	1.2
Hawes2	33.507996, -111.681884	5.2	23.7	22.2	26.7	0.0	1.1
Hawes3	33.506880, -111.679902	2.8	18.9	17.0	29.3	0.0	1.6
Hawes4	33.505153, -111.678502	2.1	31.1	27.9	22.1	0.3	0.7
Hawes5	33.503842, -111.678357	2.4	15.0	13.6	24.8	0.0	1.7
Hawes6	33.501729, -111.674401	12.5	44.2	29.9	23.0	0.9	0.5
Hawes7	33.501141, -111.671542	8.3	50.9	39.4	25.4	1.0	0.5
Hawes8	33.500904, -111.668852	27.5	47.8	36.2	23.0	1.2	0.5
Hawes9	33.500258, -111.666639	6.2	54.3	35.7	22.5	1.6	0.4
Hawes10	33.499527, -111.664402	6.6	48.0	33.4	23.9	1.2	0.5
Hawes11	33.498520, -111.662463	1.3	23.6	19.0	27.0	0.1	1.1
Hawes12	33.497179, -111.660597	0.6	22.4	20.5	26.3	0.0	1.2
Hawes13	33.496728, -111.658184	1.1	21.9	23.2	22.0	0.3	1.0
Hawes14	33.496439, -111.656003	0.8	20.0	18.6	25.9	0.2	1.3
Hawes15	33.497331, -111.654168	0.3	17.3	15.4	26.3	0.0	1.5
Las Sendas1	33.471546, -111.630903	6.0	85.0	72.3	34.8	1.5	0.4
Las Sendas2	33.473372, -111.629986	3.2	66.5	62.4	33.1	1.0	0.5
Las Sendas3	33.475454, -111.629712	2.1	52.9	50.5	35.7	0.4	0.7
Las Sendas4	33.477568, -111.629611	2.9	55.6	49.8	33.5	0.4	0.6
Las Sendas5	33.479636, -111.629675	0.2	58.7	62.0	55.3	1.6	0.9
Las Sendas6	33.481725, -111.629662	0.8	59.4	50.1	44.4	1.7	0.7
Las Sendas7	33.483831, -111.631318	1.9	67.6	61.3	49.4	1.3	0.7
Las Sendas8	33.485933, -111.632350	0.7	60.2	55.0	48.2	1.5	0.8
Las Sendas9	33.488081, -111.632870	33.0	63.6	50.9	35.0	0.2	0.6
Las Sendas10	33.490320, -111.633791	8.1	70.8	62.0	38.3	1.0	0.5
Las Sendas11	33.492553, -111.636173	7.2	64.3	49.1	36.7	7.0	0.6
Las Sendas12	33.494520, -111.636591	0.8	27.9	28.2	34.5	0.1	1.2
Las Sendas13	33.496781, -111.637449	0.2	31.1	29.6	35.2	0.2	1.1
Las Sendas14	33.497749, -111.638520	0.4	30.0	27.4	36.6	0.2	1.2

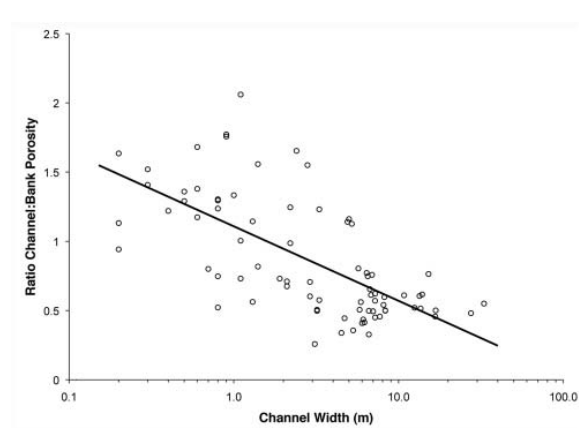


**Figure 8.** Scatterplot of all porosity sampling sites presented in Table 4. The ratio of channel porosity to bank porosity in the bedrock ( $Y$ ) is plotted against the  $\log_{10}$  of channel width ( $X$ ) with the line being the regression of  $Y = 1.099 - 0.534 \log X$ .

within the range of other locations experiencing active base-level fall; for example, in California (Riebe et al. 2000), Spain (Mather 2000; Reinhardt et al. 2007), and even tectonically active ranges (Quimet, Whipple, and Granger 2009).

A wide spectrum of erosion rates exists globally, but these comparisons serve to highlight that there is nothing unique or special about the response of this landform that has been classically considered stable to a normal geomorphic forcing such as base-level change.

It is also clear that size matters in the response of a pediment to base-level fall (Figure 7). We are struck by the planar nature of the larger Bush pediment and the Las Sendas pediment still graded to the Mesa terrace (Figure 3). The Mesa terrace was abandoned  $89.6 \pm 22.4$  ka (Table 1), and yet the Bush pediment almost completely reformed to a classic pediment transport surface within just one glacial–interglacial cycle.

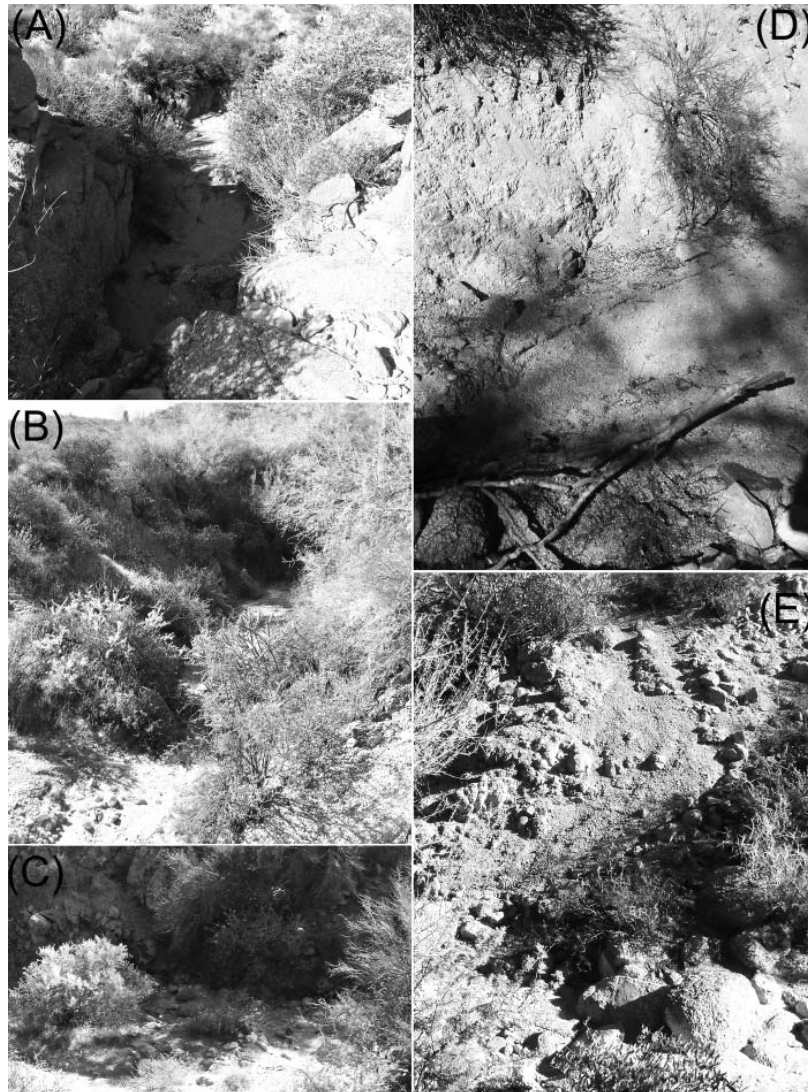


**Figure 9.** Ephemeral pediment washes where the state of granitic decay as measured by porosity varies considerably between channel bottom and banks. (A–C) Narrow incising channels where the ratio of floor to bank porosity is  $> 1$ . (D and E) The walls of widening washes where the ratio of floor to bank porosity is  $< 1$ . The state of decay of channel banks in (D) and (E) and channel floors in (A–E) can be described as strongly weathered in the classification of weathered mantles (Ehlen 2005).

### Revisiting the Role of Lateral Stream Migration

Numerous researchers once explained the planar form of pediments from lateral erosion of streams flowing across the pediment surface (Gilbert 1877; Johnson 1931, 1932; Sharp 1940; Howard 1942; Warnke 1969). Criticism of lateral erosive processes stems from the idea that drainages would have to debouche the mountain front and swing laterally, against gravity (Lustig 1969), to abut the mountain front to explain the characteristic piedmont angle (Oberlander 1989).

Opposition continues into recent modeling literature where lateral stream migration remains a relatively ignored process (Strudley, Murray, and Haff 2006; Pelletier 2010). This is despite research and observations from classic Mojave Desert pediments that 3 to 51 percent of piedmont junctions (where pediment and mountain meet) are being influenced by channel processes (Parsons and Abrahams 1984).

Based on observations made at Userly pediments, we return to the hypothesis that lateral erosion plays a pivotal role in pedimentation associated with

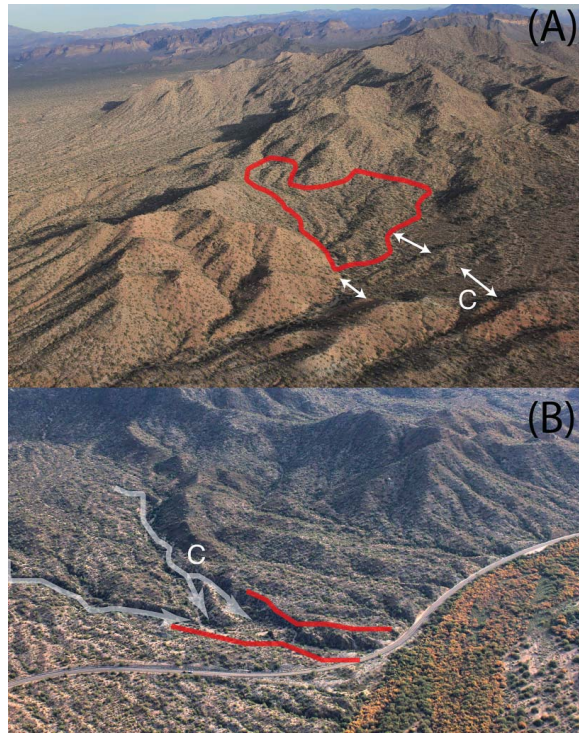


**Figure 10.** Examples of channel widening associated with larger drainage areas. (A) The Mine dissected pediment experienced drainage capture where the old channel was abandoned at C. Double arrows identify areas of channel widening associated with the larger upstream drainage area. In contrast, the polygon identifies smaller drainages that are still incising in response to the lowered base level of the Salt River. (B) The Twisted Sister dissected pediment where the solid, semitransparent arrows identify areas where the largest (in terms of drainage area) pediment ephemeral washes converge and erode laterally into relict pediment topography. Letter C identifies a location where the old channel was captured. (Color figure available online.)

adjustment to disequilibrium. The general notion of streams “avoiding” areas of less weathered granite is certainly not new, as this is a premise of stepped topography (Wahrhaftig 1965). Pelletier et al. (2009) noted this possibility also, in their model for the Catalina metamorphic core complex in Arizona, which “would yield longitudinal profiles that exhibit random walk-like behavior for snapshots in time, but knickpoints would shift laterally over time as new heterogeneities are exhumed. This point is particularly clear when considering the nature of alluvial storage in the model and in actual profiles” (382). The evidence in Table 4 and Figure 8 reveals that ephemeral wash incision occurs until the ephemeral wash encounters a resistant heterogeneity; washes then erode laterally into weaker more porous banks.

We emphasize that pediment channel widening associated with enhanced porosity might be limited to granitic lithologies that are particularly susceptible to grussification (Ehlen 2005). Because granitic pediments play a particularly important role in the pediment literature (Dohrenwend and Parsons 2009), the observations made here for the Utery pediments could have widespread applicability in interpreting pedimentation processes. Still, although the Utery granitic pediments can adjust and approach a new equilibrium condition in relatively short periods of geologic time—within just one glacial cycle—the power of base-level lowering on other rock types remains unassessed.

Research presented in small granitic ephemeral washes of the nearby South Mountains (Larson and Dorn 2014) emphasizes that a decayed condition of granitic rock facilitates lateral erosion by small ephemeral washes during flash flood events. In that study, lateral planation created strath floodplains or flat bedrock floors on which the streams operated. The similarly decayed state of granitic rock in the Utery pediments (Figure 9D–E) also facilitates lateral erosion by small pediment streams.

In the actively adjusting Utery pediments the widest portions and most significant areas of planation occur where the largest pediment drainages coalesce and in the far distal reach of the largest drainages. Figure 8 also suggests a positive relationship between pediment drainage area and the efficiency of lateral erosion. Progressive drainage capture (with examples identified in Figure 10) processes and the increased elongation of the drainages increase drainage area, allowing for adequate stream power to erode laterally in the distal portion of adjusting pediments. This adjustment and lateral planation of a new pediment surface would then proceed to more proximal reaches of the pediment over time as the pediment system evolves. We can observe this in various stages of adjustment throughout the pediments and dissected pediments in this study (Figures 4 and 10).

### The Pediment–Strath Relationship

At South Mountain, Arizona, small pediments gradually transition into strath channels that widen at the expense of the pediments during flash floods (Larson and Dorn 2014). This pediment–strath relationship also occurs in the Utery/Salt pediment system (Figure 11A). Each terrace of the Salt River is strath,

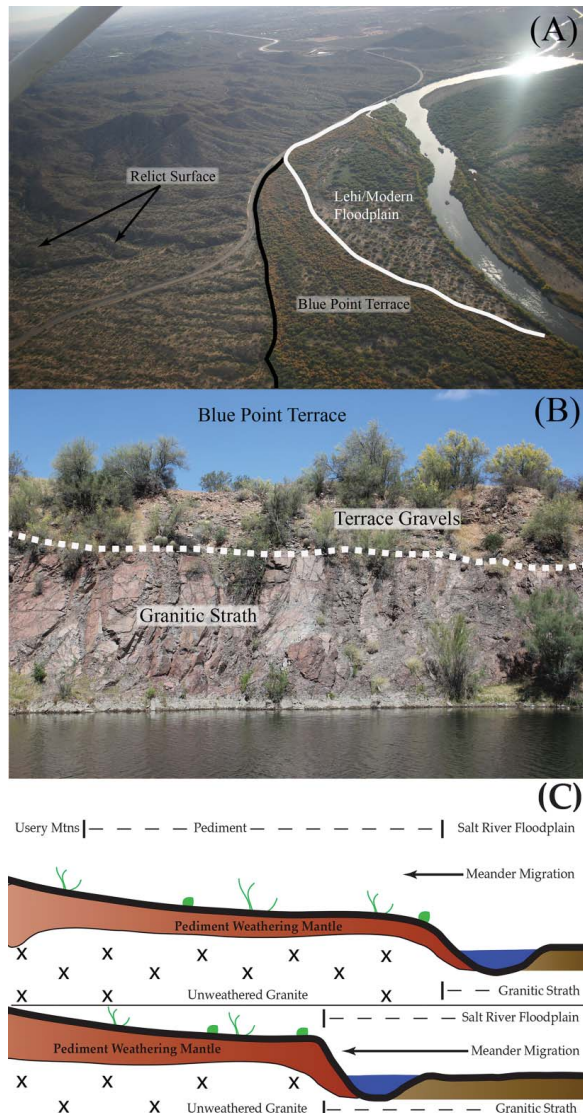


**Figure 11.** The pediment–strath relationship of the Usery pediments and the Salt River. (A) Low-level aerial photography shows the Twisted Sister pediment draining to the modern Salt River. Black arrows show the relict pediment surface that once graded to the Mesa Terrace level. The dark line indicates scarps separating the Twisted Sister pediment and the Blue Point Terrace, whereas the light line represents the scarp separating the Lehi/active floodplain level of the modern Salt from the Blue Point Terrace. Lateral migration of the Salt carved these floodplains at the expense of the bounding pediment and is continuing to do so just downstream of the Blue Point Terrace remnant picture here. (B) An exposure of Blue Point strath terrace, revealing cobbles on planed bedrock consisting of the same rock type observed making up the Usery pediments. (C) A simplified model of the pediment–strath relationship. Strath floodplains are carved at the expense of bounding pediments. When incision of the river takes place, the strath floodplain is abandoned as a strath terrace. (Color figure available online.)

consisting of the same granitic lithologies making up the adjacent pediment (e.g., Figure 11B). The Salt River’s lateral migration beveled the distal reach of the Usery pediment, creating a strath floodplain, and this appears to have occurred multiple times along the Salt River system. This likely occurs when the river is near stable conditions where longitudinal profile stability and abundant bedload on the channel floor inhibits vertical incision. Thus, stream power is not focused on the channel bed but on channel banks—in this case the flanking pediment system (Figure 11C). We hypothesize that a combination of decayed granite composing the pediment (Table 4), the weak nature of the pediment mantle cover composed of transported loose grus, wetting and drying (Montgomery 2004) of the exposed pediment along banks, and bank undercutting by floods all weaken the banks and facilitate this lateral erosion. This hypothesis could explain why all of the Salt River terrace remnants are granitic strath, many of which are isolated and surrounded by the pediment system and that pediments actively grade into these former and present strath floodplains. This relationship, originally identified by Larson and Dorn (2014), exemplifies the continuum of processes that connect the mountain-front, pediment, and base-level systems in basins of the Basin and Range. Thus, we suggest that future pediment studies attempting to understand pediment genesis look at these systems from a more complete systematic continuum as simplified in Figure 2.

## Conclusion

Toward the end of his life, the founding president of the AAG developed a passion for the genesis of beveled rock pediments in deserts (Davis 1933). A great many geographers and those in cognate disciplines have shared Davis’s passion. This contribution offers new insights to the large pediment literature regarding the importance of base level and the power of geospatial and cosmogenic nuclide methods to understand entire geomorphic systems.

Pediments of the Usery Mountains adjust to base-level fluctuations and reestablish equilibrium at rates of up to  $\sim 400$  mm/ka during the last glacial cycle. Replanation occurs through vertical stream incision into the former pediment surface, drainage capture, and lateral stream migration into weakened granitic substrates.

## Supplemental Material

Supplemental data for this article are available on the publisher's Web site at <http://dx.doi.org/10.1080/24694452.2016.1201420>

## References

- Anders, M. D., J. L. Pederson, T. M. Rittenour, W. D. Sharp, J. C. Gosse, K. E. Karlstrom, L. J. Crossey, et al. 2005. Pleistocene geomorphology and geochronology of eastern Grand Canyon: Linkages of landscape components during climate changes. *Quaternary Science Reviews* 24:2428–48.
- Anderson, R. S., J. L. Repka, and G. S. Dick. 1996. Explicit treatment of inheritance in dating depositional surfaces using in situ  $^{10}\text{Be}$  and  $^{26}\text{Al}$ . *Geology* 24:47–51.
- Applegarth, M. T. 2004. Assessing the influence of mountain slope morphology on pediment form, south-central Arizona. *Physical Geography* 25:225–36.
- Balchin, W. G. V., and N. Pye. 1956. Piedmont profiles in the arid cycle. *Proceedings of the Geologists' Association* 66:167–81.
- Balco, G., J. O. Stone, N. A. Lifton, and T. J. Dunai. 2008. A complete and easily accessible means of calculating surface exposure ages or erosion rates from  $^{10}\text{Be}$  and  $^{26}\text{Al}$  measurements. *Quaternary Geochronology* 3:174–95.
- Barsch, D., and C. F. J. Royse. 1972. A model for development of Quaternary terraces and pediment-terraces in the Southwestern United States of America. *Zeitschrift für Geomorphologie N.F.* 16:54–75.
- Bezy, J. V. 1998. The development of granite landforms on the northern and western margins of the Santa Catalina Mountains, Arizona. PhD dissertation, University of Arizona, Tucson, Arizona.
- Bierman, P. R., and M. Caffee. 2001. Slow rates of rock surface erosion and sediment production across the Namib Desert and escarpment, Southern Africa. *American Journal of Science* 301:326–58.
- Bierman, P. R., R. Coppersmith, K. Hanson, J. Neveling, E. W. Portenga, and D. H. Rood. 2014. A cosmogenic view of erosion, relief generation, and the age of faulting in southern Africa. *GSA Today* 24 (9): 4–11.
- Biro, P., and J. Dresch. 1966. Pediments and glacia in Western United-States. *Annales De Geographie* 75:513–52.
- Block, J. 2007. *3-D visualization for water resources planning and for Salt River paleo-geomorphology in central Arizona*. Tempe: Arizona State University School of Earth and Space Sciences.
- Bryan, K. 1925. The Papago Country, Arizona. U.S. Geological Survey Water Supply Paper 499. Washington, DC: U.S. Geological Survey.
- . 1940. The retreat of slopes. *Annals of the Association of American Geographers* 30:254–68.
- Büdel, J. 1982. *Climatic geomorphology*, trans. L. Fischer and D. Busche. Princeton, NJ: Princeton University Press.
- Butzer, K. W. 1965. Desert landforms at the Kurkur Oasis, Egypt. *Annals of the Association of American Geographers* 55:578–91.
- Chmeleff, J., F. von Blanckenburg, K. Kossert, and D. Jakob. 2010. Determination of the  $^{10}\text{Be}$  half-life by multicollector ICP-MS and liquid scintillation counting. *Nuclear Instruments and Methods in Physics Research Section B: Beam Interactions with Materials and Atoms* 268:192–99.
- Churchill, R. R. 1981. Aspect-related differences in badlands slope morphology. *Annals of the Association of American Geographers* 71:374–88.
- Cockburn, H. A. P., M. A. Seidl, and M. A. Summerfield. 1999. Quantifying denudation rates on inselbergs in the central Namib Desert using in situ-produced cosmogenic  $^{10}\text{Be}$  and  $^{26}\text{Al}$ . *Geology* 27:399–402.
- Cooke, R. U. 1970a. Morphometric analysis of pediments and associated landforms in the western Mojave Desert, California. *American Journal of Science* 269:26–38.
- . 1970b. Stone pavements in deserts. *Annals of the Association of American Geographers* 60:560–77.
- Cooke, R. U., and A. Warren. 1973. *Geomorphology in deserts*. Berkeley: University of California Press.
- Daly, R. A. 1944. Biogeographical memoir of William Morris Davis 1850–1934. *National Academy of Sciences of the United States of America Biographical Memoirs* 23:263–303.
- Davis, W. M. 1902. Baselevel, grade, and peneplain. *Journal of Geology* 10:77–111.
- . 1933. Granitic domes of the Mohave Desert, California. *Transactions of the San Diego Society of Natural History* 7:211–58.
- . 1938. Sheetfloods and streamfloods. *Geological Society of America Bulletin* 49:1337–1416.
- Davis, W. M., and W. H. Snyder. 1898. *Physical geography*. Boston: Ginn.
- Denny, C. S. 1967. Fans and pediments. *American Journal of Science* 265:81–105.
- DiBiase, R. A. 2014. Earth science: River incision revisited. *Nature* 505:294–95.
- Dohrenwend, J. C., and A. J. Parsons. 2009. Pediments in arid environments. In *Geomorphology of desert environments*, ed. A. J. Parsons and A. D. Abrahams, 377–411. New York: Springer.
- Dorn, R. I. 1995. Digital processing of back-scatter electron imagery: A microscopic approach to quantifying chemical weathering. *Geological Society of America Bulletin* 107:725–41.
- Douglass, J., N. Meek, R. I. Dorn, and M. W. Schmeckle. 2009. A criteria-based methodology for determining the mechanism of transverse drainage development, with application to southwestern USA. *Geological Society of America Bulletin* 121:586–98.
- Ehlen, J. 2005. Above the weathering front: Contrasting approaches to the study and classification of weathered mantle. *Geomorphology* 67:7–21.
- Ehlen, J., and E. Wohl. 2002. Joints and landform evolution in bedrock canyons. *Transactions of the Japanese Geomorphological Union* 23 (2): 237–55.
- Finnegan, N. J., R. Schumer, and S. Finnegan. 2014. A signature of transience in bedrock river incision rates over timescales of 104–107 years. *Nature* 505:391–94.
- Fisher, A., D. Fink, J. Chappell, and M. Melville. 2014.  $^{26}\text{Al}/^{10}\text{Be}$  dating of an aeolian dust mantle soil in

- western New South Wales, Australia. *Geomorphology* 219:201–12.
- Friend, D. A. 2000. Revisiting William Morris Davis and Walther Penck to propose a general model of slope “evolution” in deserts. *The Professional Geographer* 52:164–78.
- Gallen, S. F., F. J. Pazzaglia, K. W. Wegmann, J. L. Pederson, and T. W. Gardner. 2015. The dynamic reference frame of rivers and apparent transience in incision rates. *Geology* 43:623–26.
- Gilbert, G. K. 1877. *Geology of the Henry Mountains*. Washington, DC: U.S. Geological and Geographical Survey.
- Goossens, D. 1995. Field experiments of aeolian dust accumulation on rock fragment substrata. *Sedimentology* 42:391–402.
- Gran, K. B., N. Finnegan, A. L. Johnson, P. Belmont, C. Wittkop, and T. Rittenour. 2013. Landscape evolution, valley excavation, and terrace development following abrupt postglacial base-level fall. *Geological Society of America Bulletin* 125:1851–64.
- Gunnell, Y., R. Braucher, D. Bourles, and G. Andre. 2007. Quantitative and qualitative insights into bedrock landform erosion on the South Indian craton using cosmogenic nuclides and apatite fission tracks. *Geological Society of America Bulletin* 2007:576–85.
- Guralnik, B., A. Matmon, Y. Avni, and D. Fink. 2010. <sup>10</sup>Be exposure ages of ancient desert pavements reveal Quaternary evolution of the Dead Sea drainage basin and rift margin tilting. *Earth and Planetary Science Letters* 290:132–41.
- Heimsath, A. M., J. Chappell, W. E. Dietrich, K. Nishiizumi, and R. Finkel. 2001. Late Quaternary erosion in southeastern Australia: A field example using cosmogenic nuclides. *Quaternary International* 83–85: 169–85.
- Heisinger, B., D. Lal, P. Kubik, S. Ivy-Ochs, K. Knie, and E. Nolte. 2002. Production of selected cosmogenic radionuclides by muons: 2. Capture of negative muons. *Earth and Planetary Science Letters* 200:357–69.
- Heisinger, B., D. Lal, P. Kubik, S. Ivy-Ochs, S. Neumaier, K. Knie, V. Lazarev, and E. Nolte. 2002. Production of selected cosmogenic radionuclides by muons: 1. Fast muons. *Earth and Planetary Science Letters* 200:345–55.
- Holzner, L., and G. D. Weaver. 1965. Geographic evaluation of climatic and climato-genetic geomorphology. *Annals of the Association of American Geographers* 55:592–602.
- Howard, A. D. 1942. Pediment passes and pediment problem. *Journal of Geomorphology* 5:3–32, 95–136.
- Huang, W. L., X. P. Yang, A. Li, J. A. Thompson, and L. Zhang. 2014. Climatically controlled formation of river terraces in a tectonically active region along the southern piedmont of the Tian Shan, NW China. *Geomorphology* 220:15–29.
- Ives, R. L. 1936. Desert floods in the Sonoyta Valley. *American Journal of Science* 32:349–60.
- Jessup, B. S., W. J. Hahm, S. N. Miller, J. W. Kirchner, and C. S. Riebe. 2011. Landscape response to tipping points in granite weathering: The case of stepped topography in the Southern Sierra Critical Zone Observatory. *Applied Geochemistry* 26:548–50.
- Jessup, R. W. 1960. The stony tableland soils of the southeastern portion of the Australian arid zone and their evolutionary history. *Journal of Soil Science* 11:188–96.
- Johnson, D. W. 1931. Planes of lateral corrasion. *Science* 73:174–77.
- . 1932. Rock planes in arid regions. *Geographical Review* 22:656–65.
- Jungers, M. C., and A. M. Heimsath. 2015. Post-tectonic landscape evolution of a coupled basin and range: Pinaleno Mountains and Safford Basin, southeastern Arizona. *Geological Society of America Bulletin* 128 (3–4): 469–86.
- Kesel, R. H. 1977. Some aspects of the geomorphology of inselbergs in central Arizona, USA. *Zeitschrift fur Geomorphologie* 21:119–46.
- Kim, D. E., Y. B. Seong, J. M. Byun, J. Weber, and K. Min. 2016. Geomorphic disequilibrium in the Eastern Korean Peninsula: Possible evidence for reactivation of a rift-flank margin? *Geomorphology* 254:130–45.
- King, L. C. 1949. The pediment landform: Some current problems. *Geological Magazine* 86:245–50.
- Kirkby, A., and M. J. Kirkby. 1974. Surface wash at the semi-arid break in slope. *Zeitschrift fur Geomorphologie Supplementband* 21:151–76.
- Kohl, C. P., and K. Nishiizumi. 1992. Chemical isolation of quartz for measurement of in-situ produced cosmogenic nuclides. *Geochimica et Cosmochimica Acta* 56:3583–87.
- Kokalis, P. G. 1971. Terraces of the lower Salt River Valley, Arizona. In *Geology*, 103. Tempe: Arizona State University.
- Korschinek, G., A. Bergmaier, T. Faestermann, U. C. Gerstmann, K. Knie, G. Rugel, A. Wallner, et al. 2010. A new value for the half-life of <sup>10</sup>Be by heavy-ion elastic recoil detection and liquid scintillation counting. *Nuclear Instruments and Methods in Physics Research Section B: Beam Interactions with Materials and Atoms* 268:187–91.
- Koschmann, A. H., and G. F. Loughlin. 1934. Dissected pediments in the Magdalena District, New Mexico. *Geological Society of America Bulletin* 48:463–78.
- Lal, D. 1991. Cosmic ray labeling of erosion surfaces: In situ nuclide production rates and erosion models. *Earth and Planetary Science Letters* 104:424–39.
- Larson, P. H., and R. I. Dorn. 2014. Strath development in small-arid watersheds: Case study of South Mountain, Sonoran Desert, Arizona. *American Journal of Science* 314:1202–23.
- Larson, P. H., R. I. Dorn, J. Douglass, B. F. Gootee, and R. Arrowsmith. 2010. Stewart Mountain Terrace: A new Salt River terrace with implications for landscape evolution of the lower Salt River Valley, Arizona. *Journal of the Arizona-Nevada Academy of Science* 42:26–36.
- Larson, P. H., R. I. Dorn, R. E. Palmer, Z. Bowles, E. Harrison, S. Kelley, M. W. Schmeckle, and J. Douglass. 2014. Pediment response to drainage basin evolution in south-central Arizona. *Physical Geography* 35:369–89.

- Liu, B., F. M. Phillips, M. M. Pohl, and P. Sharma. 1996. An alluvial surface chronology based on cosmogenic  $^{36}\text{Cl}$  dating, Ajo Mountains (Organ Pipe Cactus National Monument), Southern Arizona. *Quaternary Research* 45:30–37.
- Lustig, L. K. 1969. Trend-surface analysis of the Basin and Range Province, and some geomorphic implications. U.S. Geological Survey Professional Paper 500-D. Washington, DC: U.S. Geological Survey.
- Mabbutt, J. A. 1966. Mantle-controlled planation of pediments. *American Journal of Science* 264:78–91.
- . 1977. *Desert landforms*. Canberra: Australian National University Press.
- . 1979. Pavements and patterned ground in the Australian stony deserts. *Stuttgarter Geographische Studien* 93:107–23.
- Mammerickx, J. 1964. Quantitative observations on pediments in the Mojave and Sonoran deserts (southwestern United States). *American Journal of Science* 262:417–35.
- Marchetti, D. W., and T. E. Cerling. 2005. Cosmogenic  $^3\text{He}$  exposure ages of Pleistocene debris flows and desert pavements in Capitol Reef National Park, Utah. *Geomorphology* 67:423–35.
- Mather, A. E. 2000. Adjustment of a drainage network to capture induced base-level change: An example from the Sorbas Basin, SE Spain. *Geomorphology* 34:271–89.
- Matmon, A., A. Mushkin, Y. Enzel, T. Grodek, and ASTER Team. 2013. Erosion of a granite inselberg, Gross Spitzkoppe, Namib Desert. *Geomorphology* 201:52–59.
- Matmon, A., O. Simhai, R. Amit, I. Haviv, N. Porat, E. McDonald, L. Benedetti, and R. Finkel. 2009. Desert pavement-coated surfaces in extreme deserts present the longest-lived landforms on Earth. *Geological Society of America Bulletin* 209:688–97.
- McFadden, L. D., S. G. Wells, and M. J. Jercinovich. 1987. Influences of eolian and pedogenic processes on the origin and evolution of desert pavements. *Geology* 15: 504–06.
- Menges, C. M., and P. A. Pearthree. 1989. Late Cenozoic tectonism in Arizona and its impact on regional landscape evolution. *Arizona Geological Society Digest* 17:649–80.
- Montgomery, D. R. 2004. Observations on the role of lithology in strath terrace formation and bedrock channel width. *American Journal of Science* 304: 454–76.
- Moss, J. H. 1977. Formation of pediments: Scarp back-weathering or surface downwasting? In *Geomorphology in arid regions*, ed. D. O. Doehring, 51–78. Binghamton, NY: 8th Annual Geomorphology Symposium.
- Nichols, K. K., P. R. Bierman, M. C. Eppes, M. Caffee, R. Finkel, and J. Larsen. 2005. Late Quaternary history of the Chemehuevi Mountain piedmont, Mojave Desert, deciphered using  $^{10}\text{Be}$  and  $^{26}\text{Al}$ . *American Journal of Science* 305:345–68.
- Nishiizumi, K., M. Imamura, M. W. Caffee, J. R. Southon, R. C. Finkel, and J. McAninch. 2007. Absolute calibration of  $^{10}\text{Be}$  AMS standards. *Nuclear Instruments and Methods in Physics Research Section B: Beam Interactions with Materials and Atoms* 258:403–13.
- Oberlander, T. M. 1972. Morphogenesis of granite boulder slopes in the Mojave Desert, California. *Journal of Geology* 80:1–20.
- . 1974. Landscape inheritance and the pediment problem in the Mojave Desert of Southern California. *American Journal of Science* 274:849–75.
- . 1979. Superposition of alluvial fans over pediments in the Mojave Desert, California. Paper presented at the Association of American Geographers Annual Meeting, Philadelphia, PA.
- . 1989. Slope and pediment systems. In *Arid zone geomorphology*, ed. D. S. G. Thomas, 56–84. London: Belhaven.
- Oliver, M. A., and R. Webster. 1990. Kriging: A method of interpolation for geographical information systems. *International Journal of Geographical Information Systems* 4:313–32.
- Ongley, E. D. 1974. Fluvial morphometry on the Cobar Pediplain. *Annals of the Association of American Geographers* 64:281–92.
- Oskin, M., L. Perg, D. Blumentritt, S. Mukhopadhyay, and A. Iriondo. 2007. Slip rate of the Calico fault: Implications for geologic versus geodetic rate discrepancy in the Eastern California Shear Zone. *Journal of Geophysical Research* 112:B03402.
- Ouimet, W. B., K. X. Whipple, and D. E. Granger. 2009. Beyond threshold hillslopes: Channel adjustment to base-level fall in tectonically active mountain ranges. *Geology* 37:579–82.
- Owen, L. A., K. Frankel, J. R. Knott, S. Reynhout, R. C. Finkel, J. F. Dolan, and J. Lee. 2011. Beryllium-10 terrestrial cosmogenic nuclide surface exposure dating of Quaternary landforms in Death Valley. *Geomorphology* 125:541–57.
- Palm, W. J. 1986. Some important aspects of the morphological processes in the southwestern United States. *Papeles de geografía* 11:63–70.
- Parsons, A. J., and A. D. Abrahams. 1984. Mountain mass denudation and piedmont formation in the Mojave and Sonoran Deserts. *American Journal of Science* 284:255–71.
- Parsons, A. J., A. D. Abrahams, and J. R. Simanton. 1992. Microtopography and soil-surface materials on semi-arid piedmont hillslopes, southern Arizona. *Journal of Arid Environments* 22:107–15.
- Pearthree, P. A., B. F. Gootee, S. M. Richrad, and J. E. Spencer. 2015. Geological map compilation for aggregate resource assessment in the Phoenix metropolitan area. Arizona Geological Survey Digital Information Series DI-43. [http://repository.azgs.gov/sites/default/files/dlio/files/nid1640/phoenixareaaggregate\\_di-43\\_simplified\\_map.pdf](http://repository.azgs.gov/sites/default/files/dlio/files/nid1640/phoenixareaaggregate_di-43_simplified_map.pdf) (last accessed 15 April 2016).
- Pelletier, J. D. 2010. How do pediments form? A numerical modeling investigation with comparison to pediments in southern Arizona, USA. *Bulletin of the Geological Society of America* 122:1815–29.
- Pelletier, J. D., M. Cline, and S. B. DeLong. 2007. Desert pavement dynamics: Numerical modeling and field-based calibration. *Earth Surface Processes and Landforms* 32:1913–27.

- Pelletier, J. D., T. Engelder, D. Comeau, A. Hudson, M. Leclerc, A. Youberg, and S. Diniega. 2009. Tectonic and structural control of fluvial channel morphology in metamorphic core complexes: The example of the Catalina-Rincon core complex, Arizona. *Geosphere* 5:363–84.
- Péwé, T. L. 1978. Guidebook to the geology of central Arizona. Arizona Bureau of Geology and Mineral Technology Special Paper 2. Phoenix: State of Arizona.
- Pietrasiak, N., R. E. Drenovsky, L. S. Santiago, and R. C. Graham. 2014. Biogeomorphology of a Mojave Desert landscape—Configurations and feedbacks of abiotic and biotic land surfaces during landform evolution. *Geomorphology* 206:23–36.
- Plakht, J., N. Patyk-Kara, and N. Gorelikova. 2000. Terrace pediments in Makhtesh Ramon, central Negev, Israel. *Earth Surface Processes and Landforms* 25:29–30.
- Pope, C. W. 1974. Geology of the lower Verde river valley, Maricopa County, Arizona. Master's thesis, Arizona State University, Tempe, AZ.
- Powell, J. W. 1875. *Exploration of the Colorado River of the West and its tributaries: Explored in 1869, 1870, and 1872 under the direction of the secretary of the Smithsonian Institution*. Washington, DC: U.S. Government Printing Office.
- Rahn, P. H. 1967. Sheetfloods, streamfloods, and formation of pediments. *Annals of the Association of American Geographers* 57:593–604.
- Reinhardt, L. J., P. Bishop, T. B. Hoey, T. J. Dempster, and D. C. W. Sanderson. 2007. Quantification of the transient response to base-level fall in a small mountain catchment: Sierra Nevada, southern Spain. *Journal of Geophysical Research Earth Surface* 112: F03S05. doi: 10.1029/2006JF000524
- Riebe, C. S., J. W. Kirchner, D. E. Granger, and R. C. Finkel. 2000. Erosional equilibrium and disequilibrium in the Sierra Nevada, inferred from cosmogenic <sup>26</sup>Al and <sup>10</sup>Be in alluvial sediment. *Geology* 28:803–06.
- Rognon, P. 1967. Climatic influences on the African Hoggar during the Quaternary, based on geomorphologic observations. *Annals of the Association of American Geographers* 57:117–27.
- Ruhe, R. V. 1964. Landscape morphology and alluvial deposits in southern New Mexico. *Annals of the Association of American Geographers* 54:147–59.
- Schmidt, K.-H. 1989. Talus and pediment flatirons erosional and depositional features on dryland cuesta scarps. *Catena Supplement* 14:107–18.
- Schumm, S. A. 1962. Erosion on miniature pediments in Badlands National Monument, South Dakota. *Bulletin of the Geological Society of America* 73:719–24.
- Sharon, D. 1962. On the nature of hamadas in Israel. *Zeitschrift für Geomorphologie N.F.* 6:129–47.
- Sharp, R. P. 1940. Geomorphology of the Ruby-East Humboldt Range, Nevada. *Bulletin of the Geological Society of America* 51:337–72.
- Skotnicki, S. J., and R. S. Leighty. 1997. Geological map of the Stewart Mountain Quadrangle, Maricopa County, Arizona. Arizona Geological Survey Open File Report 97-12. [http://repository.azgs.gov/sites/default/files/dlio/files/nid816/ofr97-12\\_stewartmntn.pdf](http://repository.azgs.gov/sites/default/files/dlio/files/nid816/ofr97-12_stewartmntn.pdf) (last accessed 15 April 2016).
- Springer, M. E. 1958. Desert pavement and vesicular layer of some soils of the desert of the Lahontan Basin, Nevada. *Proceedings of the Soil Science Society America* 22:63–66.
- Stone, J. O. 2000. Air pressure and cosmogenic isotope production. *Journal of Geophysical Research* 105:B23753–59.
- Strudley, M. W., and A. B. Murray. 2007. Sensitivity analysis of pediment development through numerical simulation and selected geospatial query. *Geomorphology* 88:329–51.
- Strudley, M. W., A. B. Murray, and P. K. Haff. 2006. Emergence of pediments, tors, and piedmont junctions from a bedrock weathering-regolith thickness feedback. *Geology* 34:805–08.
- Tator, B. A. 1952. Pediment characteristics and terminology. *Annals of the Association of American Geographers* 42:295–317.
- Tuan, Y.-F. 1962. Structure, climate and basin landforms in Arizona and New Mexico. *Annals of the Association of American Geographers* 52:51–68.
- Twidale, C. R. 1967. Hillslopes and pediments in the Flinders Range, South Australia. In *Landform studies from Australia and New Guinea*, ed. J. N. Jennings and J. A. Mabbutt, 95–117. Canberra, Australia: ANU Press.
- . 1982. *Granite landforms*. Amsterdam: Elsevier.
- . 1983. Pediments, peneplains, and ultiplains. *Revue du Geomorphologie Dynamique* 32:1–38.
- Twidale, C. R., and J. A. Bourne. 2013. Do pediplains exist? Suggested criteria and examples. *Zeitschrift für Geomorphologie* 57:411–28.
- Twidale, C. R., and J. E. Mueller. 1988. Etching as a process of landform development. *The Professional Geographer* 40:379–91.
- Wahrhaftig, C. 1965. Stepped topography of the Southern Sierra Nevada. *Geological Society of America Bulletin* 76:1165–90.
- Wakatsuki, T., Y. Sasaki, Y. Tanaka, and Y. Matsukura. 2007. Predictive equation of unit weights, shear strength parameters and permeability of grus using a simplified dynamic cone penetrometer hardness and grain size. *Journal of the Japan Society of Erosion Control Engineering* 59:38–46.
- Warnke, D. A. 1969. Pediment evolution in the Halloran Hills, Central Mojave Desert. *Zeitschrift für Geomorphologie N.F.* 13:357–89.
- Wells, S. G., J. C. Dohrenwend, L. D. McFadden, B. D. Turin, and K. D. Mahrer. 1985. Late Cenozoic landscape evolution on lava flow surfaces of the Cima volcanic field, Mojave Desert, California. *Geological Society of America Bulletin* 96:1518–29.
- Wells, S. G., L. D. McFadden, J. Poths, and C. T. Olinger. 1995. Cosmogenic <sup>3</sup>He surface-exposure dating of stone pavements: Implications for landscape evolution in deserts. *Geology* 23:613–16.
- Whipple, K. X. 2004. Bedrock rivers and the geomorphology of active orogens. *Annual Review of Earth and Planetary Sciences* 32:151–85.

PHILLIP H. LARSON is an Assistant Professor and Director of Earth Science Programs in the Department of Geography at Minnesota State University, Mankato, MN 56001.

E-mail: phillip.larson@mnsu.edu. His research interests lie in geomorphology, landscape evolution, and Quaternary environments.

SCOTT B. KELLEY is Lecturer in the School of Geographical Sciences and Urban Planning at Arizona State University, Tempe, AZ 85282. E-mail: sbkelley@asu.edu. His research interests lie in GIS, transportation geography, and sustainable energy resources and systems.

RONALD I. DORN is a Professor of Geography in the School of Geographical Sciences and Urban Planning at

Arizona State University, Tempe, AZ 85282. E-mail: atrid@asu.edu. His research interests lie in geomorphology, rock art conservation, petroglyph analysis, quantification and geography of mineral weathering, geographic education, tyranny of the majority in science, and rock coatings.

YEONG BAE SEONG is an Associate Professor of Geography in the Department of Geography Education, Korea University, Seoul, Republic of Korea. E-mail: ybseong@korea.ac.kr. His research interests lie in geomorphology and geochronologic dating methods.